Experimental and Theoretical Mechanistic Investigation on the Catalytic CO_2 Hydrogenation to Formate by a Carboxylate-functionalized bis(N-heterocyclic carbene) Zwitterionic Iridium(I) Compound

Raquel Puerta-Oteo,[†,‡] Markus Hölscher,[‡,*] M. Victoria Jiménez,[†] Walter Leitner,[‡,*] Vincenzo Passarelli, [†,§] and Jesús J. Pérez-Torrente[†,*]

[†] Departamento de Química Inorgánica, Instituto de Síntesis Química y Catálisis Homogénea–ISQCH, Universidad de Zaragoza–CSIC, Facultad de Ciencias, C/ Pedro Cerbuna, 12, 50009 Zaragoza, Spain

[‡] Institut für Technische und Makromolekulare Chemie, RWTH Aachen University, Worringerweg 2, D-52074 Aachen, Germany

[§] Centro Universitario de la Defensa, Ctra. Huesca s/n, ES–50090 Zaragoza, Spain

KEYWORDS: *CO_2 hydrogenation, Formic acid, Homogeneous catalysis, bis-NHC ligands, iridium*

ABSTRACT: The bis-imidazolium salt, 1,1-bis(N-methylimidazolium) acetate bromide, is a convenient precursor for the synthesis of zwitterionic iridium(I) [Ir(cod){(MeIm)$_2$CHCOO}] and cationic iridium(III) [IrH(cod){(MeIm)$_2$CHCOO}]$^+$ compounds (MeIm = 3-methylimidazol-2-yliden-1-yl) having a carboxylate-functionalized bis(NHC) ligand. The [Ir(cod){(MeIm)$_2$CHCOO}] compound catalyzes the hydrogenation of CO_2 to formate in water using NEt_3 as base reaching turnover numbers of approximately 1500. Reactivity studies have shown that activation of the catalyst precursor involves the reaction with H_2 in a multistep process that result, under catalytic conditions, in the formation of a dihydrido iridium(III) octahedral [IrH$_2$(H$_2$O){(MeIm)$_2$CHCOO}] species stabilized by the κ^3-*C,C',O* coordination of the ligand. DFT studies on the mechanism were carried out to elucidate two possible roles of the base. In the first one, NEt_3 neutralizes only the produced formic acid whereas in the second it assists the proton transfer in heterolytic cleavage of the H_2 molecule. Although this base-involved mechanism is more favourable exhibiting a lower energy span for the overall reaction, the energy barrier obtained from kinetic experiments suggests that both mechanisms could be operative under the experimental reaction conditions.

INTRODUCTION

Formic acid, the simplest carboxylic acid, is commonly found in nature in the bites and stings of insects. As industrial chemical it is produced mainly from methyl formate generated by carbonylation of methanol. It is also a by-product of petroleum refining (naphtha partial oxidation), biomass processing, and several industrial organic syntheses. In addition to its applications in agriculture and in the textile and leather industries, formic acid has been proposed as an energy carrier (formic acid fuel cells) and also as a potential chemical hydrogen storage system.[1,2] The use of CO_2 as a C1 feedstock for producing fuels and chemicals is an attractive strategy that potentially may be helpful in the reduction of the carbon footprint at the interface of the chemistry and energy sectors.[3] Consequently, intensive research efforts have been devoted to the search of efficient catalysts for formic acid production *via* hydrogenation of carbon dioxide.[4,5] In particular, organometallic complexes of the late transition metals have shown catalytic activity for CO_2 hydrogenation to formic acid or its derivatives such as formate salts, formamides, formate esters or silyl formats,[6] as well as in the methylation of NH bonds.[7]

The major hurdle for the direct conversion of carbon dioxide into formic acid is the combination of unfavorable reaction thermodynamics with the high kinetic stability of CO_2 toward reduction. While the hydrogenation of CO_2 in the gas phase is endergonic (ΔG^o (g) = + 7.9 kcal mol^{-1}), it is slightly exergonic in suitable solvents and in particular in aqueous phase (ΔG^o (aq) = - 1 kcal mol^{-1}).[4a,8] Using in addition a base that neutralizes the produced formic acid makes the reaction even more exergonic and drives the reaction equilibrium toward the formate salt product.[5] It has been also shown, however, that the base can participate in the catalytic cycle by assisting the heterolytic cleavage of the H_2 molecule.[9] At the same time, acid/base equilibria of CO_2 in water must be also considered for the kinetics of the transformation.[10] CO_2 reaches equilibrium with bicarbonate and carbonate under basic conditions. The equilibrium concentrations of CO_2/HCO_3^-/CO_3^{2-} are highly dependent on pH, temperature and CO_2 pressure,

and the actual reactive species may change with the reaction conditions.

Inoue *et al.* firstly reported the homogeneous catalytic hydrogenation of CO_2 into formic acid in seventies.[11] Since then, many transition-metal complexes based on ruthenium, rhodium, iridium, iron and cobalt have been extensively investigated. A common feature of most catalytic systems is that all key transformations occur at the metal center whereas the ligands act as spectators. However, in the last decade, the design of catalytic systems involving the active participation of the ancillary ligands have allowed for the development of outstandingly active catalytic systems for the reduction of CO_2.[4,12]

Himeda *et al.* developed a series of water soluble half-sandwich Cp*Ir(III) complexes having proton-responsive ligands, such as dihydroxy-substituted 2,2'-bipyridine or 1,10-phenanthroline, and a dinuclear catalyst with a tetrahydroxy-substituted bipyrimidine as a bridging ligand, which have successfully been applied to the hydrogenation of CO_2.[13] A seminal contribution was made by Nozaki *et al.* that disclose the iridium(III) [IrH_3(PNP)] catalysts featuring a pyridine-based pincer ligand (PNP = 2,6-bis(di-isopropylphosphino-methylene)pyridine) which showed very high catalytic activity for the hydrogenation of CO_2 to formate under basic conditions.[14] Subsequently, Hazari *et al.* developed a related water soluble iridium trihydride catalyst featuring a flexible pincer amine–diphosphine ligand, [IrH_3(PNP)] (PNP = $HN(C_2H_4P^iPr_2)_2$). Interestingly, the reaction proceeds through an outer-sphere mechanism in which the N-H moiety plays a crucial role.[15] A related iridium pincer catalyst featuring an imine–diphosphine ligand operating through a mechanism involving metal–imine cooperative catalysis has been recently reported by Zhou.[16]

Transition metal catalysts based on lutidine-derived pincer ligands exhibit a "non-innocent" behavior through metal–ligand cooperation involving an aromatization/dearomatization mechanism associated to H_2 activation, one of the key steps in the catalytic cycle of CO_2 hydrogenation.[17] In addition, it has been demonstrated that ruthenium complexes having lutidine-derived pincer ligands are also able to cooperatively interact with CO_2 after being dearomatized by reaction with a strong base, resulting in the formation of a M–O bond and C–C bond to the exo-cyclic methine carbon of the pincer arm.[18] However, this interaction is usually reversible and does not hamper the catalytic activity under the appropriate catalytic conditions. In fact, compound [RuH(CO)(PNN)] (PNN = 2-(di-tert-butylphosphinomethyl)-6-(diethylamino-methyl)pyridine) shows an excellent catalytic activity in the hydrogenation of CO_2 to formate.[19] Noteworthy, Pidko *et al.* reported a catalytic activity to a TOF of 1.1 10^6 h^{-1} of catalyst [RuHCl(CO)(PNP)] (PNP = 2,6-bis(di-tert-butylphosphino-methylene)pyridine) in DMF using DBU as base.[20]

N-heterocyclic carbenes (NHC) have recently attracted widespread attention in homogeneous catalysis because of their strong coordination ability and tunable character that allows for the control of the steric and electronic properties of the metal centre.[21] However, only a limited number of catalysts based on such ligands for the hydrogenation of CO_2 have been hitherto reported. Peris *et al.* disclosed the catalytic activity of a series of water-soluble ruthenium and iridium complexes having bis-NHC ligands for the reduction of CO_2 to formate with hydrogen and by transfer hydrogenation.[22] The catalytic activity for carbon dioxide hydrogenation and formic acid dehydrogenation of iridium and ruthenium complexes featuring a bidentate ligand containing a NHC and a pyridinol ring has been very recently described by Grotjahn *et al.*[23] Finally, the catalytic activity in CO_2 hydrogenation of lutidine-derived bis-N-heterocyclic carbene ruthenium CNC–pincer complexes has been studied by Pidko *et al.* They observe irreversible formation of a stable CO_2 adduct that is not catalytically competent. However, this deactivation pathway can be effectively suppressed by an increase of the H_2/CO_2 ratio resulting in a high catalytic performance.[24]

In recent years our research interest has been focused on the synthesis and catalytic applications of transition-metal complexes containing functionalized NHC ligands of hemilabile character.[25] We have now envisaged the potential of carboxylate-functionalized bis(NHC) ligands for the construction of a metal-ligand platform with application in catalysis. The carboxylate group at the linker should confer hemilabile properties to the ligands allowing for the stabilization of catalytic intermediates through the κ^3-*C,C',O*-tridentate coordination mode. The aim of this work is the preparation of a water-soluble iridium catalyst precursor comprising this principle for the hydrogenation of CO_2 in water and the investigation of the reaction mechanism by a combination of experimental and computational studies.

RESULTS AND DISCUSSION

Synthesis and reactivity of iridium complexes bearing a carboxylate-functionalized bis(NHC) ligand. The carboxylate-functionalized bis-(imidazolium) salt precursor was prepared according to the general synthetic method entailing the alkylation of N-alkylimidazole with a suitable functionalized alky bromide.[26] Thus, reaction of ethyl dibromoacetate with an excess of N-methylimidazole in THF at 343 K for 72 h gave a brown slurry from which the salt 1,1'-bis(N-methylimidazolium) acetate bromide, [$(MeImH)_2CHCOO$] Br (**1**), was obtained as a white hygroscopic solid in 79% yield after recrystallization from methanol/acetone (Scheme 1).

Scheme 1. Synthesis of 1,1-bis(N-methylimidazolium) acetate bromide.

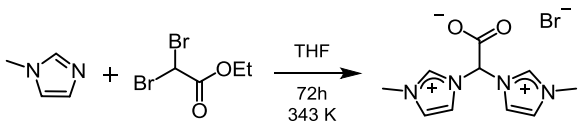

1 (79 %)

The isolation of **1** is, to certain extent, an unanticipated result because the formation of the ester functionalized bis-imidazolium salt $[(MeImH)_2CHCOOEt]Br_2$ should be expected. However, under anhydrous reaction conditions and in the presence of a large excess of bromide, nucleophilic substitution by bromide likely results in the formation of ethyl bromide and the carboxylate moiety.[27]

The salt **1** has been characterized by means of FT-IR, ^1H and $^{13}C\{^1H\}$ NMR spectroscopy, as well as mass spectrometry. Although the ESI+ mass spectrum of **1** only shows the cation fragment resulting from the decarboxylation of the compound, the ATR-IR spectrum showed two intense absorption bands at 1671 and 1367 cm^{-1} corresponding to the asymmetric and symmetric -COO stretching modes, respectively, of the carboxylate fragment. The ^1H NMR spectrum of **1** in DMSO-d_6 showed a set of five resonances in agreement with the proposed structure of C_S symmetry. The low-field shifted resonance at δ 9.50 ppm corresponds to the equivalent NC*H*N imidazolium protons whereas the C*H*COO was observed at 7.19 ppm. Interestingly, both resonances were not observed in the ^1H NMR spectrum recorded in CD_3OD as a consequence of fast H/D exchange, which is in agreement with the acid character of both types of protons. The most relevant resonances in the $^{13}C\{^1H\}$ NMR spectrum of **1** (DMSO-d_6) are those of the CHCOO fragment which were observed at δ 159.5 (COO) and 70.4 (CH) ppm, respectively.

The synthesis of the zwitterionic iridium(I) [Ir(cod){$(MeIm)_2CHCOO$}] (**2**) compound was accomplished by using the *in-situ* deprotonation of the functionalized bis-imidazolium salt methodology.[28] Thus, sequential reaction of $[(MeImH)_2CHCOO]Br$ (**1**) with half equivalent of $[Ir(\mu\text{-}OMe)(cod)]_2$ and NaH (60% oil dispersion) in MeOH gave a dark red solution from which complex **2** was isolated as a red microcystalline solid in 70% yield after removing the inorganic salts (Scheme 2). It is worth mentioning that **2** could not be prepared by reaction of **1** with NaH (2 equiv) and $[Ir(\mu\text{-}Cl)(cod)]_2$. In spite of the strict reaction conditions required for the synthesis and isolation of **2**, in particular exclusion of oxygen and moisture, the compound is soluble and stable in methanol or water under argon.

Scheme 2. Synthesis of carboxylate-functionalized bis(NHC) iridium(I) and iridium(III) complexes.

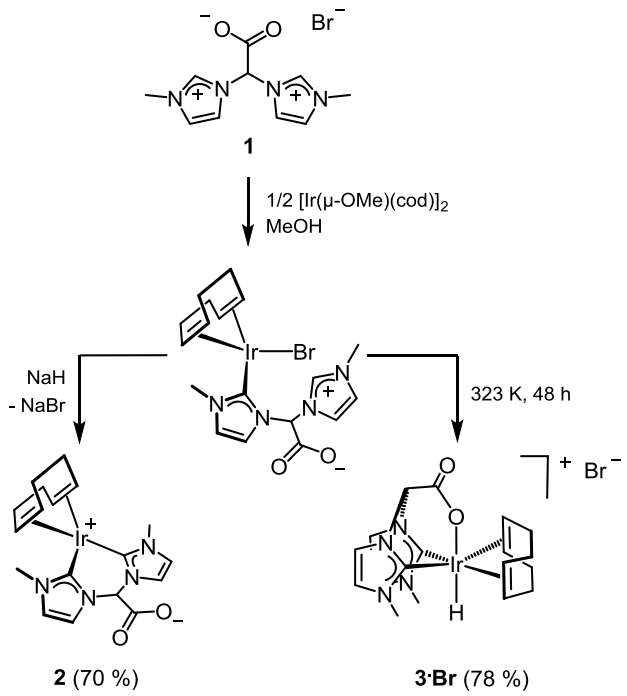

2 (70 %) **3·Br** (78 %)

The zwitterionic character for **2** was established by an X-ray diffraction analysis. The ORTEP view of the complex and selected bond lengths and angles are given in Figure 1. The complex contains a κ^2-*C,C'* coordinated bis-NHC ligand and a bidentate cod ligand resulting in a distorted square planar geometry at the metal centre. The observed angle φ = 18.6º (Figure 1b) between plane A - through Ir(1), C(1) and C(9) - and plane B - through Ir(1), centroid [C(15)-C(16)] and centroid [C(19)-C(20)] - clearly indicates a deviation from the ideal square planar geometry similar to that observed in the related cations of formula $[M(cod)(bis\text{-}NHC)]^+$ (bis-NHC = methylenebis(imidazol-2-ylidene) (M = Rh,[29] Ir[30]).

The iridium-bis-NHC metallacycle adopts a puckered conformation with a dihedral angle of 60.4º between the least square planes containing each carbene ring. Also yaw angles[29] of 6.7º and 8.3º have been observed for the C(1)- and C(9)-carbenes, respectively. The Ir(1)–C(1) and Ir(1)–C(9) bond lengths (2.048(3) and 2.036(3) Å) and the C(1)–Ir(1)–C(9) bite angle (83.57(12)º) are similar to those reported for related chelate bis-NHC iridium complexes.[30] When dealing with the carboxylato group, the C(14)–O(1) and C(14)–O(2) bond lengths (1.244(4), 1.252(4) Å) and the O(1)–C(14)–O(2) angle of 128.4(3)º are indicative of a delocalised negative charge. In addition the lattice methanol molecules are found to interact with the oxygen atoms of the carboxylate groups with O–H···O contacts of 2.7 Å (av.) and almost lineal D–H–A angles (See Supporting Information).

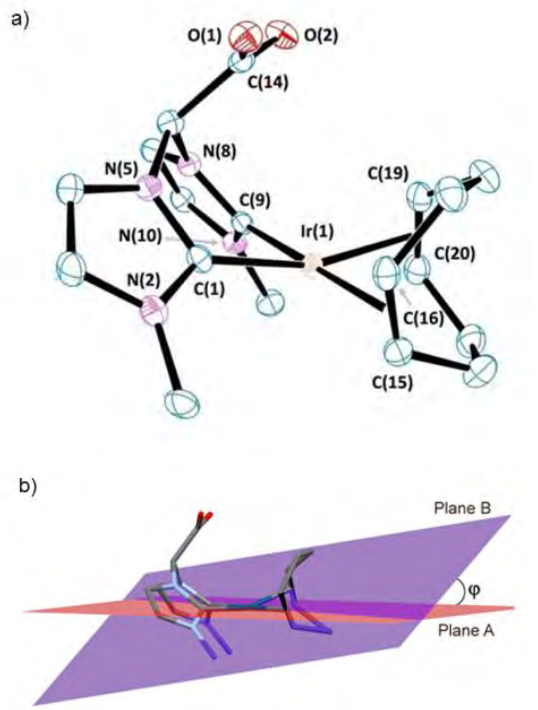

Figure 1. a) ORTEP view of [Ir(cod){(MeIm)$_2$CHCOO}] (**2**) with the numbering scheme adopted. Ellipsoids are at the 50% probability and the hydrogen atoms are omitted for clarity; b) View of the angle φ between plane A (Ir(1) C(1) C(9)) and plane B (Ir(1) centroid[C(15)-C(16)] centroid[C(19)-C(20)]). Selected bond lengths (Å) and angles (º): Ir(1)-C(1) 2.048(3), Ir(1)-C(9) 2.036(3), Ir(1)-ct(1) 2.0758(1), Ir(1)-ct(2) 2.0581(1), C(15)-C(16) 1.396(5), C(19)-C(20) 1.397(5), C(14)-O(1) 1.244(4), C(14)-O(2) 1.252(4), C(1)-Ir(1)-C(9) 83.57(12), O(1)-C(14)-O(2) 128.4(3), C(1)-Ir(1)-ct(1) 95.77(8), C(1)-Ir(1)-ct(2) 161.51(9), C(9)-Ir(1)-ct(1) 178.91(9), C(9)-Ir(1)-ct(2) 94.49(8), ct(1)-Ir(1)-ct(2) 85.86(1). ct(1): centroid[C(15)-C(16)], ct(2): centroid[C(19)-C(20)].

The ^{1}H and ^{13}C{^{1}H} NMR spectra of **2** in CD_3OD are in agreement with the molecular structure of C_s symmetry found in the solid state. The existence of the iridium–carbene bonds was confirmed by the absence of resonances for the imidazolium protons in the ^{1}H NMR spectrum and the singlet resonance observed at δ 176.25 ppm in the ^{13}C{^{1}H} NMR spectrum. In addition, the presence of two resonances at δ 4.67 and 4.42 ppm for the =CH protons of the cod ligand in the ^{1}H NMR spectrum that correlate with those at 81.4 and 75.3 ppm in the ^{13}C{^{1}H} NMR spectrum suggests a rigid boat conformation of the 6-membered metallacycle in solution.

In sharp contrast, reaction of [(MeImH)$_2$CHCOO]Br (**1**) with a suspension of [Ir(μ-OMe)(cod)]$_2$ (half equiv) in MeOH at 323 K for 48 h gave a yellow-orange suspension of the iridium(III) [IrH(cod){(MeIm)$_2$CHCOO}]Br (**3·Br**) compound which was isolated in 78% yield (Scheme 2). Most likely, the formation of **2** and **3·Br** proceeds through the common intermediate species of type [IrBr(NHC)(cod)] that results from the deprotonation of one of the imidazolium fragments in **1** by the bridging methoxo ligands of [Ir(μ-OMe)(cod)]$_2$. Further deprotonation of the pendant imidazolium fragment by NaH or NaOMe, formed by reaction of NaH with MeOH, should result in the formation of **2** after elimination of NaBr. However, in the absence of additional base the oxidative addition of the acidic C2-H of the pendant imidazolium fragment[31] affords the iridium(III)-hydrido species **3**$^+$ which was isolated as the bromide salt (Scheme 2).

The species **3**$^+$ has been characterized by multinuclear NMR spectroscopy and mass spectra (ESI+), which showed the molecular ion at m/z 521.2 with the correct isotopic distribution. In addition, the molecular structure of the triflate salt **3·OTf** has been determined by an X-ray diffraction study (see below). The ^{1}H NMR spectrum of **3·Br** in DMSO-d_6 showed a singlet at δ -19.05 ppm which is consistent with the presence of an Ir-H bond. In addition, the number of resonances in the ^{1}H and ^{13}C{^{1}H} NMR spectra suggests an octahedral structure of C_s symmetry with the symmetry plane relating both halves of the bis-NHC and cod ligands. Interestingly, the resonance for the equivalent carbene carbon atoms was observed at δ 149.6 ppm, considerably high-field shifted compared to that of **2** (176.2 ppm) likely as a consequence of the coordination to the Ir(III) centre. On the other hand, the κ^3-*C,C',O* coordination of the carboxylate-functionalized bis(NHC) ligand results in a significant down-field shift of the *CH*COO resonance at δ 6.89 ppm which is a diagnostic for this coordination mode. In the same way, the =CH resonances of the cod ligand were observed at δ 5.90 and 4.67 ppm largely down-field shifted compared to those of **2**. The hydrido ligand in **3**$^+$ undergoes fast H/D exchange in CD_3OD at room temperature suggesting an acidic character.[32]

Scheme 3. Protonation of [Ir(cod){(MeIm)$_2$CHCOO}] (**2**) by HOTf.

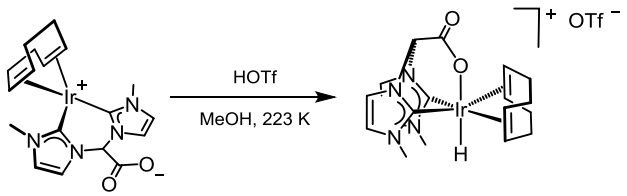

2 **3·OTf** (77 %)

Interestingly, the zwitterionic complex [Ir(cod){(MeIm)$_2$CHCOO}] (**2**) reacts with HOTf in dichloromethane at 223 K to give a yellow suspension of the salt **3·OTf** which was isolated in 77% yield (Scheme 3). The ^{1}H NMR spectra of **3·OTf** in CD_3OD (273 K) showed the characteristic singlet at δ -19.05 ppm that confirmed the formation of the iridium(III)-hydrido complex **3**$^+$. In spite of the presence of a basic uncoordinated carboxylate fragment in **2**, protonation likely takes place directly at the basic iridium centre resulting in the formation of an unsaturated square-pyramidal iridium (III) species. This

unusual geometry enforces the coordination of the carboxylate moiety to give the octahedral species with the functionalized bis-NHC ligand coordinated in *fac*-disposition.

The solid state structure of **3·OTf** was determined by single crystal X-ray diffraction. The molecular structure of the cation $[IrH(cod)\{(MeIm)_2CHCOO\}]^+$ is shown in Figure 2. The coordination polyhedron at the metal centre is a distorted octahedron. The κ^3-*C,C',O* bis-NHC ligand adopts a *fac* coordination mode and the coordination sphere is completed by the hydride ligand, trans to O(1) (H(1)–Ir(1)–O(1) 172(1)º), and the bidentate cod ligand. The bite angle C(1)–Ir(1)–C(9) (82.9(1)º) and the Ir(1)–C(1) and Ir(1)–C(9) bond lengths (2.029(3), 2.028(3) Å) are similar to those observed in the iridium(I) derivative **2**. Nevertheless, reasonably as a consequence of the κ^3-*C,C',O* coordination to the metal centre, both the dihedral angle between the least square planes containing each carbene ring (69.6º) and the yaw angles of the C(1)- and C(9)-carbene moieties (9.5º, 9.2º) are bigger than those observed for the square planar complex **2**.

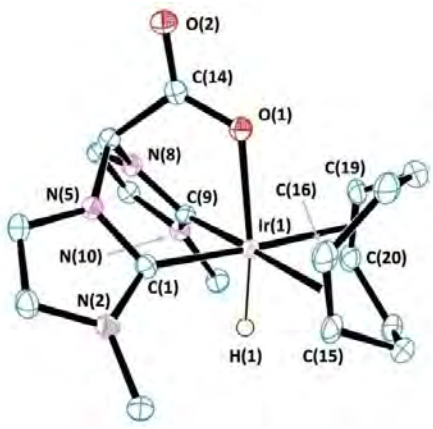

Figure 2. ORTEP view of the cation $[IrH(cod)\{(MeIm)_2CHCOO\}]^+$ in **3·OTf** with the numbering scheme adopted. Ellipsoids are at the 50% probability and the hydrogen atoms, except H(1), are omitted for clarity. Selected bond lengths (Å) and angles (º): Ir(1)-C(1) 2.029(3), Ir(1)-C(9) 2.028(3), Ir(1)-ct(1) 2.1718(1), Ir(1)-ct(2) 2.1618(1), Ir(1)-O(1) 2.188(2), Ir(1)-H(1) 1.55(2), C(15)-C(16) 1.377(4), C(19)-C(20) 1.382(4), C(14)-O(1) 1.281(3), C(14)-O(2) 1.221, C(1)-Ir(1)-C(9) 82.9(1), C(1)-Ir(1)-ct(1) 97.40(7), C(1)-Ir(1)-ct(2) 177.34(7), C(9)-Ir(1)-ct(1) 178.00(7), C(9)-Ir(1)-ct(2) 96.51(7), ct(1)-Ir(1)-ct(2) 83.323(3), O(1)-Ir(1)-H(1) 172(1), O(1)-Ir(1)-C(1) 84.67(9), O(1)-Ir(1)-C(9) 86.04(8). ct(1): centroid[C(15)-C(16)], ct(2): centroid[C(19)-C(20)].

Hydrogenation of CO_2 to formate catalyzed by $[Ir(cod)\{(MeIm)_2CHCOO\}]$ (2). The catalytic activity of the zwitterionic iridium(I) complex **2** for the hydrogenation of CO_2 was evaluated. The reactions were carried out under 60 atm of 2:1 H_2/CO_2 in a 1.8 M solution of NEt_3 in water in the presence of 0.07 mol% of iridium catalyst at 110 °C. The catalytic results obtained in the hydrogenation of CO_2 under these reaction conditions are shown in Table 1. Analysis of the final reaction solution evidenced in all cases the exclusive formation of the triethylamine/formic acid adduct as product. Conversion values were calculated from the $HCOOH/NEt_3$ ratio and the amount of base added in each experiment with the 1:1 adduct typically observed in aqueous phase defined as 100% of conversion. The values are averaged from at least two measurements with a reproducibility of ±5%. A negative mercury drop test indicated that iridium nanoparticles are not involved in the catalytic process.

Table 1. Hydrogenation of CO_2 to formate catalyzed by **2**.[a]

$$CO_2 + H_2 \xrightarrow[1.8\ M\ NEt_3/H_2O]{[Ir]} HCOO^- + HNEt_3^+$$

Entry	Cat.	T °C	t h	mmol HCOO⁻	[HCOO⁻] (M)	yield (%)	TON[b]	TOF[b]
1	**2**	110	4	3.65	0.91	51	729	182
2	**2**[c]	110	20	0.03	0.01	<1	7	0.3
3	**2**[d]	110	4	2.69	0.53	54	538	135
4	**2**[e]	110	4	2.43	0.61	34	486	121
5	**4**	110	4	2.64	0.66	37	528	132
6	**2**	110	2	2.79	0.70	39	558	279
7	**2**	110	42	7.13	1.78	99	1427	34
8	**2**	110	72	7.75	1.94	108	1550	22
9	**2**	80	20	3.96	0.99	55	791	40
10	**2**	110	20	6.40	1.60	89	1280	64
11	**2**	140	20	5.74	1.44	80	1148	57
12	**2**[f]	110	20	5.44	1.36	76	857	43

[a] Catalyst: 5 μmol, at 60 atm (PH_2/PCO_2: 2/1) in H_2O (3 mL), NEt_3 (1 ml, 7.17 mmol). [b] TONs based on formate concentration calculated by ^1H NMR in D_2O using DMF as internal standard. TOFs (h^{-1}) calculated at the end of reaction time. [c] No base. [d] KOH 1M as base (5 mL, 5 mmol). [e] DMSO as solvent. ^1H NMR in DMSO-d_6 using mesitylene as internal standard. [f] 60 atm (PH_2/PCO_2: 1/1)

Under these initial conditions catalyst precursor **2** provided a 51% yield to formate in 4 h with an average TOF of 182 h^{-1} (entry 1). The presence of the base is essential for catalysis as no significant catalytic activity was observed under the same reaction conditions in the absence of base even at longer reaction times (entry 2). The nature of the base also influences the catalytic activity. Although NEt_3 has been frequently employed as base in CO_2 hydrogenation reactions,[6a,33] a variety of bases have been also evaluated as for example K_2CO_3, KOH, K_3PO_4, or $KHCO_3$. In general, weaker bases result in lower activity and consequently KOH is one of the most used bases for this reaction.[20a,20c,22b,27b] However, a decrease of activity was observed when the hydrogenation of CO_2 was performed in a 1M KOH solution in water, under the same reactions conditions, giving a 54% of conversion but with a TOF of

135 h^{-1} (entry 3). As can be seen in Table 1, the catalytic performance of **2** was inferior in DMSO (entry 4) and consequently, NEt_3/H_2O was used as reaction medium throughout the study. Interestingly the related cationic bis-NHC iridium [Ir(cod){$(MeIm)_2CH_2$}]I (**4**) compound lacking the carboxylate functional group is less active than **2** giving a 37% yield with a TOF of 132 h^{-1} (entry 5), which suggests that the carboxylate group in the bis-NHC ligand of **2** has an important role in the catalysis. The evolution of conversion with the reaction time has been also studied showing a steady increase of the amount of formic acid produced (entries 6-8). The highest TOF of 279 h^{-1} was observed at 2 h with a 39% conversion and full conversion was attained after 42 h with an average TOF of 34 h^{-1}. Longer reaction times resulted in higher yields, which is likely due to the formation of $HCOOH/NEt_3$ with stoichiometry slightly higher than 1:1.

Previous studies have demonstrated that the catalytic productivity in the hydrogenation of CO_2 is largely dependent on the temperature.[3,4,4c] In general, the catalytic productivity expressed as the attained formate concentration increases with the temperature as in the case of the Sanford's [RuH(CO)(PNN)][19] catalyst. However, it has been found that the catalytic productivity of $[RuCl_2(PTA)_4]$[8b] decrease with temperature which probably reflects the interplay of catalyst stability and thermodynamic stability of the product. The performance of the catalyst precursor **2** has been studied in the temperature range of 80-140 ºC (entries 9-11). At 80ºC the hydrogenation proceeds up to 55% of conversion after 20h. As it could be expected, an increase of the catalytic activity was attained at 110 ºC with a 89% conversion after the same reaction time. However, a 140 ºC a slight decrease in conversion was observed, which is most likely due to catalyst deactivation. Finally, the influence of the H_2(g) partial pressure on the catalytic activity was studied. It has been found that lowering of the H_2(g) partial pressure maintaining the total pressure results in a decreased of the catalytic activity with a 76% of conversion in 20 h (entries 10 and 12) which is in agreement with the results reported by Nozaki *et al.*[14a]

In order to determine the activation parameters for the hydrogenation of CO_2 to formate catalyzed by **2**, the temperature influence on the reaction rate was further investigated. A set of catalytic experiments was performed under 60 atm of 2:1 H_2/CO_2 in a 1.8 M solution of NEt_3 in water (0.07 mol% iridium catalyst load) in the temperature range 50-110 ºC. The obtained results after two hours reaction time are summarized in Table 2. As can be seen, a steady increase in the formate yield was attained with increasing the temperature, with the largest TOF value of 279 h^{-1} at 110 ºC.

Table 2. Influence of temperature on the hydrogenation of CO_2 to formate catalyzed by **2**.[a]

Entry	Cat.	T °C	t h	mmol $HCOO^-$	[$HCOO^-$] (M)	yield (%)	TON[b]	TOF[b]
1	**2**	50	2	0.27	0.07	4	54	27
2	**2**	65	2	0.36	0.09	5	58	36
3	**2**	80	2	0.64	0.16	9	128	64
4	**2**	95	2	1.54	0.38	21	308	154
5	**2**	110	2	2.79	0.70	39	558	279

[a] Catalyst: 5 μmol, at 60 atm (PH_2/PCO_2: 2/1) in H_2O (3 mL), NEt_3 (1 ml, 7.17 mmol). [b] TONs based on formate concentration calculated by ^1H NMR in D_2O using DMF as internal standard. TOFs (h^{-1}) calculated at the end of reaction time (2 h).

TOF values determined at two hours reaction time were used to derive the activation parameters by using the logarithmic form of the Eyring equation (see Supporting Information). The kinetic parameters obtained from the Eyring plot (Figure 3) were $\Delta H^{\ddagger}$ = 9.3 (3.7) kcal mol^{-1}, $\Delta S^{\ddagger}$ = -40.1 (11.9) cal/K·mol and $\Delta G^{\ddagger}$ = 21.2 (5.2) kcal mol^{-1} at 298 K.

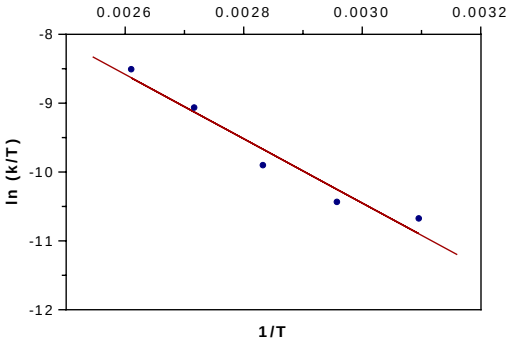

Figure 3. Eyring plot for the hydrogenation of CO_2 to formate catalyzed by **2**.

Mechanistic studies: reaction of [Ir(cod){$(MeIm)_2CHCOO$}] (2) with CO_2 and H_2. In order to gain insight into possible catalytic active species in the hydrogenation of CO_2 the reaction of **2** with carbon dioxide and hydrogen under milder conditions was explored. Stirring of a solution of [Ir(cod){$(MeIm)_2CHCOO$}] (**2**) in MeOH under a CO_2(g) atmosphere immediately resulted in a colour change from deep red to yellow. However, the solution turned out red again under vacuum suggesting that the reaction in the presence of CO_2 is a reversible process, which was confirmed by ^1H NMR analysis. Working on a concentrated suspension of **2** in MeOH (1 mL) under CO_2(g) a yellow solid could be isolated upon addition of diethyl ether. To our surprise, we found that the ^1H NMR spectrum of this solid showed exclusively the presence of the iridium(III)-hydrido species [IrH(cod){$(MeIm)_2CHCOO$}]$^+$ (**3**$^+$). We hypothesized that adventitious water in methanol could play a key role in the formation of **3**$^+$. In fact, compound **2** did not react with CO_2(g) in dichloromethane under strict anhydrous conditions. However, in agreement with our

expectations, the addition of *ca.* 1 μL of water resulted in the clean formation of $\mathbf{3}^+$. As CO_2(g) reversibly forms carbonic acid in aqueous solution and traces of water are required to perform the reaction, HCO_3^- was seen as possible counter-anion of $\mathbf{3}^+$ (Scheme 4).

Scheme 4. Reversible formation of $[IrH(cod)\{(MeIm)_2CHCOO\}]^+$ ($\mathbf{3}^+$) from **2** and CO_2(g) in the presence of water.

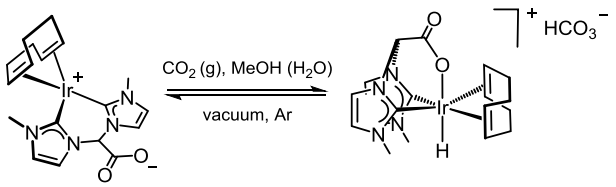

In order to confirm this proposal the reaction of **2** with isotopic labeled carbon dioxide ($^{13}CO_2$) was carried out in CD_3OD in a NMR tube equipped with a Young Valve. The ^{1}H NMR spectrum of the obtained yellow solution confirmed the formation of $\mathbf{3}^+$ and the $^{13}C\{^1H\}$ NMR spectrum showed, besides the resonance of the dissolved CO_2 at δ 126.3 ppm, a resonance at δ 161.5 ppm which was assigned to the $H^{13}CO_3^-$ anion (see Supporting Information),[35] thereby confirming the formation of $\mathbf{3}\cdot\mathbf{HCO_3}$.

Most likely the mechanism for the formation of $\mathbf{3}^+$ involves the direct protonation of the iridium centre by the carbonic acid generated under reaction conditions, pK_a = 6.35.[36] In fact, we have shown that protonation of **2** by a strong acid (HOTf) results in the clean formation of $\mathbf{3}^+$. However, the water attack to a CO_2 adduct of **2** followed by proton transfer to the iridium centre assisted by coordination of the carboxylate moiety cannot be ruled out.[37]

A suspension of $[Ir(cod)\{(MeIm)_2CHCOO\}]$ (**2**) in MeOH immediately reacted under a H_2(g) atmosphere to give a pale yellow solution that turned out into an off-white suspension in a few minutes. Unfortunately the isolated solid was completely insoluble in common organic solvents which preclude its characterization. Therefore, a variable temperature ^{1}H NMR study in CD_3OD was carried out in order to identify possible reaction intermediates.

As soon as the argon atmosphere was changed by dihydrogen immediate reaction between **2** and H_2(g) was observed even at 213 K. The ^{1}H NMR spectrum at 213 K in the hydride region showed the presence of two main species. The first one displays two resonances at δ -10.75 and -13.69 ppm, which showed correlation peaks in the ^{1}H-^{1}H-cosy NMR spectrum, which were assigned to the zwitterionic iridium (III) dihydride species $[IrH_2(cod)\{(MeIm)_2CHCOO\}]$ (**5**). In agreement with the unsymmetrical structure of **5** the spectrum shows four resonances in the range δ 4.82-4.08 ppm for the inequivalent =CH protons of the cod ligand. The second species displays a single resonance at δ -24.40 ppm and was assigned to the species $[IrH(1\text{-}\kappa\text{-}4,5\text{-}\eta\text{-}C_8H_{13})\{(MeIm)_2CHCOO\}]$ (**6**) having a σ,π-cyclooctenyl ligand resulting from the insertion of the coplanar C=C bond of the cod ligand in **5** into the Ir-H bond (Scheme 5).[38,39] Increasing the temperature to 233 K caused a broadening for the hydrido resonances of **5** and an increase in the intensity of the hydrido resonance of **6** (see Supporting Information). In fact, complete disappearance of **5** took place at 248 K. Interestingly, a new species featuring two hydrido doublet resonances at δ -10.03 and -30.52 ppm ($J_{H\text{-}H}$ = 6.1 Hz) appeared at 253 K which was supposed to be the dihydrido species $[IrH_2(coe)\{(MeIm)_2CHCOO\}]$ (**7**) (Scheme 5). The small value of the $J_{H\text{-}H}$ coupling constant is indicative of a mutually cis disposition of both hydrido ligands. In addition, the spectrum showed four resonances for the imidazole-2-carbene ring protons and other two for the =CH protons of the coe ligand at δ 4.83 and 4.10 ppm, which is consistent with an unsymmetrical structure with the hydrido ligands having very different trans ligands. The hydrido ligand at δ -10.03 should be located trans to the carbenic atom carbon whereas the high-field shifted resonance at -30.52 ppm should correspond to the hydrido ligand trans to the carboxylate moiety of the functionalized bis-NHC ligand κ^3-*C,C',O* coordinated.[40] The mechanism for the formation of **7** likely involves reductive elimination in **6** to give a cyclooctene-iridium(I) intermediate (not observed) that further reacts with dihydrogen to give the dihydrido species. However, heterolytic hydrogenolysis of the Ir-C bond in **6** with assistance of the carboxylate group followed by protonation of the resulting Ir(I) centre could also lead to the formation of **7**.

At this point it is worth of note that the above mentioned off-white solid was formed from 248 K upwards along with formation of cyclooctene. Finally, increasing the temperature to 293 K resulted in the disappearance of **6**. Thus, the off-white solid possibly could be a polymeric species that results from the elimination of coe from **7**.

Scheme 5. Hydrido species identified in the reaction of $[Ir(cod)\{(MeIm)_2CHCOO\}]$ (**2**) with H_2(g) in the temperature range of 213-293 K.

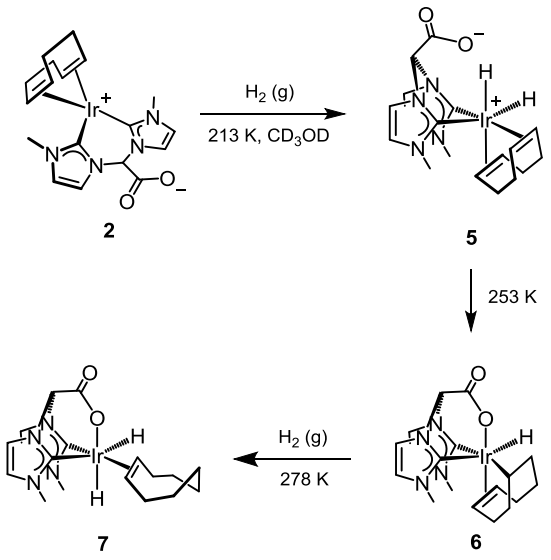

Theoretical calculations on the CO_2 hydrogenation mechanism. The above described results reveal the ability of the carboxylate-funcionalized bis-NHC ligand to stabilize iridium(III) octahedral species through the κ³-*C,C',O* coordination mode. On the other hand, the electron rich iridium centre in [Ir(cod){(MeIm)$_2$CHCOO}] (**2**) promotes the activation of dihydrogen and the hydrogenation of the coordinated 1,5-cyclooctadiene to cyclooctene which has proven to be a labile ligand.[41] Thus, under the catalytic reaction conditions (H_2O, 60 atm, PH_2/PCO_2: 2/1) replacement of the coe ligand in **7** by a water molecule to give the species [$IrH_2(H_2O)$}{(MeIm)$_2$CHCOO}] (**A**) can be assumed. In order to shed light on the reaction mechanism, a computational study at the DFT level has been carried out. In the following discussion all the energies are reported in terms of Δ*G* (kcal mol^{-1}). The optimized structure of **A** is octahedral with the iridium (III) metal centre surrounded by the functionalized bis-NCH ligand with a κ³-*C,C',O* facial coordination, two hydride ligands mutually cis disposed and trans to the carboxylate and imidazole-2-carbene fragments, and a water molecule trans to the remaining imidazole-2-carbene fragment, in full agreement to the experimentally observed complex **7**.

We have considered three mechanisms. The first one relies on the active participation of the base in bond forming/bond breaking chemical events. The second one is a mechanism in which the base only deprotonates the formed formic acid thus creating the necessary driving force for the reaction.[9] Thirdly, a mechanism with the participation of HCO_3^- was investigated.

At first the mechanism involving the assistance of the amine in the proton transfer during heterolytic cleavage of the H_2 molecule is described (Figure 4). In this pathway, the activation of H_2 precedes the CO_2 insertion.

Replacement of the water molecule by a hydrogen molecule in the catalytic active species [$IrH_2(H_2O)$}{(MeIm)$_2$CHCOO}] (**A**) is by and large energy neutral (Δ*G* = -1.0 kcal mol^{-1}) and gives the octahedral dihydride-dihydrogen complex **B** with the dihydrogen ligand *trans* to one of the imidazole-2-carbene fragments. Heterolytic cleavage of the coordinated dihydrogen molecule by NEt_3, via $\mathbf{TS_{BC}}$ with an energy barrier of 5.4 kcal mol^{-1}, gives the anionic trihydride iridium (III) species **C** which is 6.6 kcal mol^{-1} more stable than **B**. Association of CO_2 at **C** leads to minimum **D**, with the CO_2 molecule showing no significant interaction with the metal complex. From **D**, CO_2 insertion into a Ir-H bond through a transition state $\mathbf{TS_{DE}}$ ($\Delta G^{\ddagger}$ = +9.2 kcal mol^{-1}) gives the formate complex **E**, which is 11.6 kcal mol^{-1} more stable than **B**. The intermediate **E** features a formate molecule coordinated to the iridium center and hydrogen bonded to the $HNEt_3^+$ cation. In a further step, replacement of the formate product by a water molecule results in the regeneration of the catalytic active species **A'** and the release of the formate product as an acid-base adduct.

NEt_3 and HCOOH are known to form relatively stable adducts ranging from 1:1, 1:2 or 2:5 ratios.[42] Here, the determination of the end point energy was calculated assuming the formation of a 1:1 acid-base adduct. In terms of energy, this base-involved reaction pathway shows an energy span of the overall reaction of $\Delta G^{\ddagger}$ = 16.2 kcal mol^{-1} with the turn over determining intermediate being **E** (-12.6 kcal mol^{-1}) and the turn over determining transition state being $\mathbf{TS_{BC}}$ (4.4 – 0.8 = 3.6 kcal mol^{-1}) suggesting that the reaction should proceed even at room temperature.

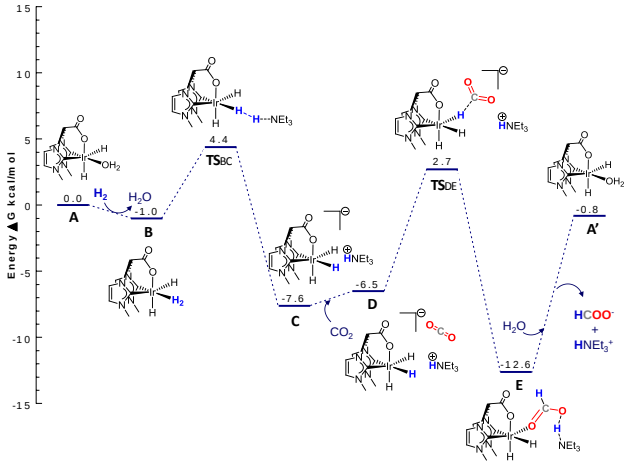

Figure 4. DFT calculated Gibbs free energy profile for the hydrogenation of CO_2 catalyzed by [$IrH_2(H_2O)$}{(MeIm)$_2$CHCOO}] in water via amine-assisted heterolytic H_2 cleavage (base-involved mechanism).

In an alternative base-free catalytic cycle a low energy transition state could be identified in which the catalytic reduction of carbon dioxide starts by insertion of CO_2 into the iridium-hydride bond as depicted in Figure 5.[19,43]

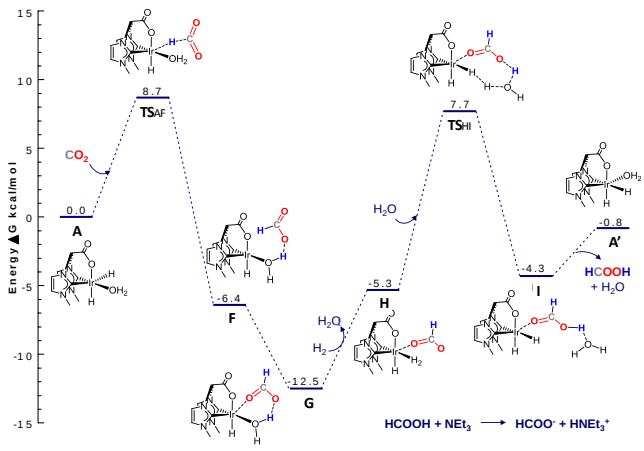

Figure 5. DFT calculated Gibbs free energy profile for the hydrogenation of CO_2 catalyzed by $[IrH_2(H_2O)\{(MeIm)_2CHCOO\}]$ in water via water-assisted heterolytic H_2 cleavage (base-free mechanism).

CO_2 insertion takes place by an outer sphere mechanism that entails the nucleophilic attack of the hydride ligand *trans* to the imidazole-2-carbene fragment to a CO_2 molecule. Passing through transition state $\mathbf{TS_{AF}}$ with an energy barrier of 8.7 kcal mol^{-1}, the hydride is transferred directly from the iridium center to the carbon atom in CO_2 to form the formate complex **F**. This intermediate, where the formate remains loosely bonded to the coordinated water molecule is more stable than **A** by 6.4 kcal mol^{-1}. This intermediate rearranges to intermediate **G** in which the formate molecule weakly interacts with the iridium center through the C=O bond while maintaining the interaction with the coordinated water molecule. These interactions provide an energy minimum more stable than **A** by 12.5 kcal mol^{-1}. Stabilization of formate by hydrogen bonding has been reported by several authors, suggesting that solvation effect by H_2O decrease the energy barrier for the insertion of CO_2 in the M-H bond.[43d,44]

Proton transfer from **G** to the coordinated formate is possible once the water molecule is replaced by H_2 generating **H** which is uphill by 7.2 kcal mol^{-1}.[45] Proton transfer from **H** to the oxygen atom of the formate is mediated by an external water molecule through $\mathbf{TS_{HI}}$ with an energy barrier of 13.0 kcal mol^{-1} (Figure 6). The heterolytic cleavage of the dihydrogen molecule results in the formation of the dihydride species **I** having a solvated formic acid molecule coordinated to the iridium center which is 4.3 kcal mol^{-1}more stable than **A**. Attempts to find an alternative $\mathbf{TS_{HI}}$ where the proton is transferred directly from the dihydrogen molecule to the oxygen atom of the formate were unsuccessful despite intensive research. In the last step of the catalytic cycle, formic acid is dissociated from the iridium complex and neutralized by the base to form the acid-base adduct $[HNEt_3^+–HCOO^-]$ with regeneration of the catalytic active species **A'**. It should be noted, that in water a stabilization of formic acid by the base is not inevitably necessary as the Gibbs free energy of the formation of formic acid from CO_2/H_2 was computed to be -1.6 kcal/mol (see Supporting Information). The seemingly counterintuitive fact that the stabilization by water solely is stronger than by the base can be debilitated by the facts that i) the computed 1:1 Hbase$^+$HCOO$^-$ adduct might not be exactly what is present in solution and ii) that hydrogen bonding plays a more prominent role in the solvent water than can be described by using an implicit solvation model.

In this mechanism the energy span defining intermediate is **G** (-12.5 kcal mol^{-1}) and the transition state with the highest energy is $\mathbf{TS_{AF}}$ (8.7 – 0.8 = 7.9 kcal mol^{-1}), which gives an overall activation barrier for the reaction of $\Delta G^{\ddagger}$ = 20.4 kcal mol^{-1} (12.5 + 7.9 kcal mol^{-1}) and thus, the rate-determining transition state for this pathway is the attack of the hydride to CO_2 in $\mathbf{TS_{AF}}$. In pure water the computed Gibbs free overall activation barrier $\Delta G^{\ddagger}$ is 19.6 kcal/mol.

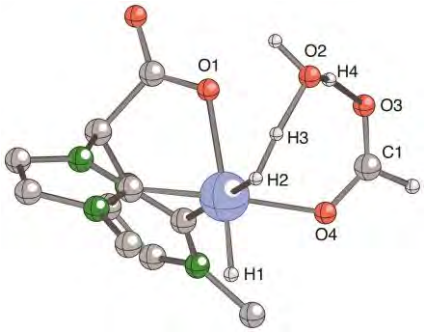

Figure 6. Structure of $\mathbf{TS_{HI}}$. Optimized geometry of $\mathbf{TS_{HI}}$ with selected atom distances (Å): Ir-O1 2.232, Ir-H1 1.597, Ir-H2 1.740, H2-H3 0.971, H3-O2 1.301, O2-H4 0.989, H4-O3 1.707, O3-C1 1.236, C1-O4 1.256.

Catalytic tests in the absence of base do show catalytic activity (Table 1, entry 2), albeit with only very limited product formation. This supports the finding that the reaction mechanism shown in Figure 5 is catalytically competent.

The computed energy spans for both mechanisms agree sufficiently well with the experimental value obtained from kinetic experiments. However, due to a non negligible error in the experimental value ($\Delta G^{\ddagger}$ = 21.2 (±5.2) kcal mol^{-1}) a clear distinction between the two mechanisms basing on energy differences only is not possible. Accordingly, both mechanisms should in principle be operative under the experimental reaction conditions.

In order to explore the possible participation of hydrogen carbonate in the catalytic reaction the reactivity of the catalytic active species $[IrH_2(H_2O)\{(MeIm)_2CHCOO\}]$ (**A**) with HCO_3^- was studied by DFT calculations. HCO_3^- can be protonated by the coordinated water molecule of **A** through a transition state in which the simultaneous breaking of C-O bond results in the formation of CO_2, water and the anionic hydroxo $[IrH_2(OH)\{(MeIm)_2CHCOO\}]^-$ complex. The high energy

barrier of 26.5 kcal mol^{-1} for this process along with the possible subsequent insertion of CO_2 into the Ir-OH bond to give stable carbonate species,[46] that likely is not competent for catalysis, allow to discard this reaction pathway. Furthermore, transfer of a hydride from **A** to HCO_3^- with simultaneous formation of formate and hydroxide also is not possible due to an even higher barrier (see Supporting Information).

CONCLUSIONS

The zwitterionic iridium(I) [Ir(cod){$(MeIm)_2CHCOO$}] and cationic iridium(III) $[IrH(cod)\{(MeIm)_2CHCOO\}]^+$ compounds having a carboxylate-functionalized bis(NHC) ligand have been prepared from the salt 1,1-bis(N-methylimidazolium) acetate bromide. The carboxylate moiety, that remains uncoordinated in the iridium(I) compound, allows the stabilization of the iridium(III)-hydrido compound through the coordination to the iridium center resulting in a κ^3-*C,C',O*-tridentate facial coordination mode.

The [Ir(cod){$(MeIm)_2CHCOO$}] compound catalyzes the hydrogenation of CO_2 to formate in water using NEt_3 as base. Reactivity studies have evidenced that activation of the catalyst precursor involves the reaction with H_2 followed by the hydrogenation of the cod ligand in a multistep process that results, under catalytic conditions, in the likely formation of the dihydrido iridium(III) species $[IrH_2(H_2O)\{(MeIm)_2CHCOO\}]$. In agreement with this, the related bis-NHC iridium $[Ir(cod)\{(MeIm)_2CH_2\}]^+$ compound lacking the carboxylate functional group showed inferior catalytic performance.

DFT studies on the reaction mechanism have shown that two mechanistic scenarios are plausible: a) A mechanism in which the base participates in the heterolytic cleavage of a coordinated dihydrogen molecule in the species $[IrH_2(H_2)\{(MeIm)_2CHCOO\}]$. This mechanism is more favourable in terms of energy with a lower energy span for the overall reaction. b) The catalytic reduction of carbon dioxide involving the insertion of CO_2 into an iridium-hydride bond of $[IrH_2(H_2O)\{(MeIm)_2CHCOO\}]$ which is followed by proton transfer to the coordinated formate through the heterolytic cleavage of the dihydrogen mediated by an external water molecule. In both cases formic acid is neutralized by the base to form an acid-base adduct. However, according to the calculations an entirely base free mechanism in which formic acid is relased directly can also be operative, which is reflected by the finding that small amounts of formic acid were detected in a base free experiment. The computed energy span for both mechanisms agrees sufficiently well with the experimental value obtained from kinetic experiments and thus, both mechanisms could be operative under the experimental reaction conditions.

EXPERIMENTAL SECTION

General Considerations. All the experimental procedures were performed under an argon atmosphere using Schlenk or glovebox techniques. Solvents were taken under argon atmosphere from an Innovative Technologies PS-400-6 solvent purification system (SPS), or dried following standard procedures and distilled under argon prior to use. Standard literature procedures were used to prepare the starting materials $[Ir(\mu\text{-}Cl)(cod)]_2$,[47] $[Ir(\mu\text{-}OMe)(cod)]_2$[48] and $[(MeIm)_2CH_2]I_2$.[49] 1-Methylimidazole (MeImH) and ethyl dibromoacetate were obtained from Aldrich and Alfa Aesar, respectively, and used as received. Deuterated solvents CD_3OD, CD_2Cl_2 and DMSO-d_6 were dried with molecular sieves and degassed by repeated freeze-pump-thaw cycles. NMR spectra were recorded on Bruker Avance 300MHz, Bruker ARX 300 or Bruker Avance 400 MHz spectrometers. Chemical shifts are reported in ppm (parts per million) and referenced relative to residual peaks of the deuterated solvent. Coupling constants *J* are given in Hertz. Full assignment of the resonances was done by combination of ^1H-^1H gradient-selected correlation spectroscopy (COSY), ^1H-^{13}C heteronuclear single quantum coherence (HSQC) and ^1H-^{13}C heteronuclear multiple bond correlation (HMBC). Mass spectra and high-resolution mass spectra were obtained on a Bruker Esquire3000 plus™ ion-trap mass spectrometer equipped with a standard ESI source. Infrared spectra were recorded on a 100 FTIR-Perkin-Elmer Spectrophotometer equipped with a Universal Attenuated Total Reflectance (UATR) accessory made by thallium bromide-iodide crystals (KRS-5). Elemental analyses for C, H, and N were carried out in a PerkinElmer 2400 Series II CHNS/O analyser.

Synthesis of 1,1'-bis(N-methylimidazole) acetate bromide, [$(MeIm)_2CHCOO$]Br (1). Ethyl dibromoacetate (0.5 mL, ρ = 1.902 $g{\cdot}mL^{-1}$, 3.86 mmol) and N-methylimidazole (1.0 mL, ρ = 1.03 $g{\cdot}mL^{-1}$, 12.50 mmol) were dissolved in THF (4 mL) into a Teflon-sealed glass vessel and the solution stirred at 343 K for 72 hours. After cooling to room temperature the brown solid residue was dissolved in methanol and the solution concentrated to *ca.* 5 mL. Addition of acetone (10 mL) gave the salt as white solid that was filtered, washed with acetone (3 x 10 mL) and dried under vacuum. Yield: 915 mg, 79%. ^1H NMR (298 K, 300 MHz, DMSO-d_6): δ 9.48 (s, 2H, NCHN), 7.92 (t, $J_{H\text{-}H}$ = 1.8, 2H, CH), 7.74 (t, $J_{H\text{-}H}$ = 1.8, 2H, CH), 7.16 (s, 1H, C*H*COO), 3.89 (s, 6H, NCH_3). $^{13}C\{^1H\}$ NMR (298 K, 75 MHz, DMSO-d_6): δ 159.5 (COO), 137.9 (C_{NCN}), 123.5, 122.0 (CH), 70.4 (*C*HCOO), 36.1 (NCH_3). MS (ESI+, MeOH, *m/z*, %): 177.3 ($[(MeIm)_2CH]^+$, 75), 95.6 ($[MeImCH]^+$, 33). IR (ATR, cm^{-1}): 1671 (COO). Anal. Calc. for $C_{10}H_{13}BrN_4O_2$: C, 39.88; H, 4.35; N, 18.60. Found: C, 39.57; H, 4.57; N, 18.48.

Synthesis of [Ir(cod){$(MeIm)_2CHCOO$}] (2). $[Ir(\mu\text{-}OMe)(cod)]_2$ (114.7 mg, 0.173 mmol) was added to a solution of [$(MeIm)_2CHCOO$]Br (**1**) (103.9 mg, 0.345 mmol) in MeOH (5 mL) to give a yellow suspension which was stirred for 30 min. Then, NaH (15.2 mg, 60% oil dispersion, 0.380 mmol) was added to give immediately a dark red solution which was stirred for 4 hours at room temperature. The solution was concentrated to *ca*. 1 mL under

reduced pressure to give a red microcrystalline solid which was filtered, washed with cold methanol (2 x 1 mL) and dried under vacuum. Yield: 125.5 mg, 70%. ^{1}H NMR (298 K, 400 MHz, CD_3OD): δ 7.40 (d, J_{H-H} = 2.0, 2H, CH), 7.14 (d, J_{H-H} = 2.0, 2H, CH), 6.38 (s, 1H, C*H*COO), 4.67 (m, 2H, =CH cod), 4.42 (m, 2H, =CH cod), 3.77 (s, 6H, NCH_3), 2.46-2.33 (br m, 4H, $>CH_2$ cod), 2.17-2.12 (br m, 2H, $>CH_2$ cod), 1.72-1.64 (br m, 2H, $>CH_2$ cod). $^{13}C\{^1H\}$ NMR (298 K, 101 MHz, CD_3OD): δ 176.2 (C_{NCN}), 170.1 (COO), 123.1, 122.7 (CH), 81.4 (=CH cod), 76.3 (*C*HCOO), 75.3 (=CH cod), 38.0 (NCH_3), 32.5, 31.2 ($>CH_2$ cod). MS (ESI^+, MeOH, *m*/*z*, %): 553.1 ($[M + H + MeOH]^+$, 57), 537.1 ($[M + OH]^+$, 100), 521.2 ($[M + H]^+$, 26). IR (ATR, cm^{-1}): 1648 (COO). Anal. Calc. for $C_{18}H_{23}IrN_4O_2$: C 41.61; H, 4.46; N, 10.78. Found: C 41.61; H, 4.59; N, 10.44. Suitable crystals for X-ray diffraction analysis were grown by slow evaporation of a concentrated solution of the complex in methanol.

[IrH(cod){(MeIm)$_2$CHCOO}]Br (3·Br). [(MeIm)$_2$CH COO]Br (**1**) (127.0 mg, 0.422 mmol) was disolved in MeOH (10 mL) into a Teflon-sealed glass vessel and then [Ir(μ-OMe)(cod)]$_2$ (139.8 mg, 0.211 mmol) was added. The suspension was stirred for two days at 323 K to give a yellow-orange suspension which was concentrated to ca. 2 mL and filtered off via cannula. The yellow solid was washed with diethyl ether (3 x 5 mL) and dried under vacuum. Yield: 197.5 mg, 78%. ^{1}H NMR (298 K, 300 MHz, DMSO-d_6): δ 7.77 (d, J_{H-H} = 1.9, 2H, CH), 7.43 (d, J_{H-H} = 1.9, 2H, CH), 6.89 (s, 1H, C*H*COO), 5.90 (m, 2H, =CH cod), 4.67 (m, 2H, =CH cod), 3.73 (s, 6H, NCH_3), 2.77-2.57 (m, 4H, $>CH_2$ cod), 2.48-2.40 (m, 2H, $>CH_2$ cod), 2.33-2.17 (m, 2H, $>CH_2$ cod), -19.05 (s, 1H, Ir-H). $^{13}C\{^1H\}$ NMR (298 K, 75 MHz, DMSO-d_6): δ 163.8 (COO), 149.6 (C_{NCN}), 124.3, 121.0 (CH), 96.3, 93.6 (=CH cod), 73.2 (*C*HCOO), 38.4 (NCH_3), 31.7, 27.0 ($>CH_2$ cod). MS (ESI+, DMSO/MeOH, *m*/*z*, %): 521.2 ($[M]^+$, 100). Anal. Calc. for $C_{18}H_{24}BrIrN_4O_2$: C, 36.00; H, 4.03; N, 9.33. Found: C, 36.08; H, 4.01; N, 9.36. IR (ATR, cm^{-1}): 2216 (Ir-H), 1654 (COO).

Synthesis of [IrH(cod){(MeIm)$_2$CHCOO}]OTf (3·OTf). HOTf (5.0 μL, ρ = 1.69 $g\cdot mL^{-1}$, 0.056 mmol) was added to a red suspension of [Ir(cod){(MeIm)$_2$CHCOO}] (**2**) (29.1 mg, 0.056 mmol) in CH_2Cl_2 (3 mL) at 223 K to give a yellow suspension in 10 minutes. The solvent was removed under vacuum to give a yellow solid, which was washed with diethyl ether (3 x 3 mL) and dried in vacuo. Yield: 28.8 mg, 77%. ^{1}H and $^{13}C\{^1H\}$ NMR data (298 K, 300 MHz, DMSO-d_6) evidenced the formation of the cation $[IrH(cod)\{(MeIm)_2CHCOO\}]^+$. MS (ESI+, DMSO/MeOH, *m*/*z*, %): 521.2 ($[M]^+$, 100). Anal. Calc. for $C_{19}H_{24}F_3IrN_4O_5S$: C 34.08; H, 3.61; N, 8.37; S, 4.79. Found: C, 34.02; H, 3.60; N, 8.39; S, 4.81. IR (ATR, cm^{-1}): 2224 (Ir-H), 1658 (COO), 1000. Suitable crystals for X-ray diffraction analysis were grown by slow evaporation of a concentrated solution of the complex in methanol.

Synthesis of [Ir(cod){(MeIm)$_2$CH$_2$}]I (4). The compound was prepared following the procedure described by Herrmann *et al*. for the rhodium complex [Rh(cod){(MeIm)$_2$CH$_2$}]I.[50] NaH (12.1 mg, 95% oil dispersion, 0.480 mmol) and [Ir(μ-Cl)(cod)]$_2$ (73.2 mg, 0.109 mmol) were dissolved independently in ethanol (5 mL) and the solutions combined and stirred for 30 minutes. The clear yellow solution was added via cannula to a solution of [(MeIm)$_2$CH$_2$]I$_2$ in ethanol (5 mL) to give a dark orange suspension. Stirring for 4 h gave an orange solution which was concentrated to *ca.* 1 mL under reduced pressure. Slow addition of cold diethyl ether (3 mL) afforded an orange solid which was filtered, washed with diethyl ether (3 x 3 mL) and dried in vacuo. Yield: 83.2 mg, 63%. ^{1}H NMR (298 K, 400 MHz, CD_2Cl_2): δ 7.26 (d, J_{H-H} = 2.0, 2H, CH), 6.81 (d, J_{H-H} = 2.0, 2H, CH), 6.03 (d, J_{H-H} = 11.9, 1H, NCH_2N), 5.82 (d, J_{H-H} = 11.9, 1H, NCH_2N), 3.82 (m, 4H, =CH cod), 3.79 (s, 6H, NCH_3), 2.32-2.06 (m, 4H, $>CH_2$ cod), 2.01-1.80 (m, 4H, $>CH_2$ cod). $^{13}C\{^1H\}$ NMR (298 K, 101 MHz, CD_2Cl_2): δ 172.1 (C_{NCN}), 122.2, 119.2 (CH), 63.8 (=CH cod) and (NCH_2N), 39.3 (NCH_3), 33.2 ($>CH_2$ cod). MS (ESI^+, MeOH, *m*/*z*, %): 477.16 ($[M]^+$, 100). Anal. Calc for $C_{17}H_{24}IIrN_4$: C 33.83; H, 4.01; N, 9.28. Found: C, 33.92; H, 4.40; N, 9.01.

Reaction of [Ir(cod){(MeIm)$_2$CHCOO}] (2) with CO$_2$. A low pressure/vacuum (LPV) 5 mm NMR tube equipped with a Young valve was charged with a suspension of [Ir(cod){(MeIm)$_2$CHCOO}] (**2**) (12.0 mg, 0.023 mmol) in CD_3OD (0.4 mL). The red suspension was frozen and the argon atmosphere changed by carbon dioxide to give immediately a clear yellow solution. The ^{1}H NMR spectrum revealed the formation of $[IrH(cod)\{(MeIm)_2CHCOO\}]^+$ (**3**$^+$). The $^{13}C\{^1H\}$-apt spectrum of the solution obtained using isotopic labelled carbon dioxide ($^{13}CO_2$) showed a resonance at δ 161.46 ppm which was assigned to the $H^{13}CO_3^-$ anion.[35]

Reaction of [Ir(cod){(MeIm)$_2$CHCOO}] (2) with H$_2$. A low pressure/vacuum (LPV) 5 mm NMR tube equipped with a Young valve was charged with a solution of [Ir(cod){(MeIm)$_2$CHCOO}] (**2**) (12.0 mg, 0.023 mmol) in CD_3OD (0.4 mL). The red suspension was frozen and the argon atmosphere changed by dihydrogen. A variable-temperature NMR study in the range 213-293 K was undertaken. Selected ^{1}H NMR data for the identified species:

[IrH$_2$(cod){(MeIm)$_2$CHCOO}] (**5**). ^{1}H NMR (213 K, 300 MHz, CD_3OD): δ 7.71 (s, CH), 7.44 (s, CH), 7.33 (s, CH), 6.94 (s, CH), 6.55 (s, C*H*COO), 4.82 (br, =CH cod), 4.61 (br, =CH cod), 4.50 (br, =CH cod), 4.08 (br, =CH cod), 3.82 (s, NCH_3), 3.80 (s, NCH_3), -10.75 (s, 1H, Ir-H), -13.69 (s, 1H, Ir-H).

[IrH(1-κ-4,5-h-C_8H_{13}){(MeIm)$_2$CHCOO}] (**6**). ^{1}H NMR (248 K, 300 MHz, CD_3OD): δ 7.52 (d, J_{H-H} = 1.7, CH), 7.46 (d, J_{H-H} = 1.5, CH), 7.23 (d, J_{H-H} = 1.7, CH), 7.04 (d, J_{H-H} = 1.5, CH), 6.48 (s, C*H*COO), 5.66 (br, =CH), 4.59 (br, =CH) (C_8H_{13}), 3.75 (s, NCH_3), 3.65 (s, NCH_3), -24.40 (s, 1H, Ir-H).

[IrH$_2$(coe){(MeIm)$_2$CHCOO}] (**7**). ^{1}H NMR (298 K, 300 MHz, CD_3OD): δ 7.60 (d, J_{H-H} = 1.8, CH), 7.48 (d, J_{H-H} = 1.9, CH), 7.24 (d, J_{H-H} = 1.8, CH), 7.15 (d, J_{H-H} = 1.9, CH), 6.53 (s, 1H, C*H*COO), 4.83 (br, =CH coe), 4.10 (br, =CH coe), 3.74 (s, NCH_3), 3.58 (s, NCH_3), -10.07 (d, J_{H-H} = 5.8, 1H, Ir-H), -30.55 (d, J_{H-H} = 6.1, 1H, Ir-H).

General Procedure for catalytic CO$_2$ hydrogenation experiments. All high-pressure batch catalytic experi-

ments were carried out in a stainless steel autoclave equipped with a 20 mL glass cylinder and a magnetic stir bar. After sealing, the reactor was deoxygenated several times by evacuation-refill (argon) cycles. A solution of the catalyst precursor (0.005 mmol) in 3 mL of degassed water and 1 mL NEt_3 was transferred to the reactor under argon via teflon cannula. The autoclave was pressurized with CO_2 to 20/30 bar and then H_2 was added up to a total pressure of 60 bar. The reaction mixture was vigorously stirred and heated in an oil bath at 353-413 K for the appropriate reaction time. Thereafter, the autoclave was cooled in an ice bath, the unreacted gases carefully released and the reaction solution analysed by ^{1}H NMR with DMF (dimethylformamide) as internal standard. TONs were found to be reproducible within ± 5% from two or three independent runs for selected experiments.

Computational details. DFT calculations performed in this work were carried out with the Gaussian09 program (revision D.01).[51] All structures were calculated with the MN12-L functional[52] and the def2-TZVP[53] basis set in combination with the associated ECP for iridium.[54] The automatic density fitting approximation was activated.[55] To account for solvent effects the solvent water was implicitly included in the geometry optimizations by applying the IEF-PCM, SMD solvation model.[56] An elevated pressure was specified to take entropy effects of the solvent into account (1354 atm).[57] The resulting structures were classified as minima or transition states by frequency calculations showing no (i = 0) or 1 (i = 1) imaginary frequency for local minima and transition states, respectively. Thermal corrections were calculated for a temperature of 298 K. For some compounds mentioned in Figure S6 of the supporting information the def2-TZVPD basis set was used for optimizations/energy computations to properly describe anionic systems. Besides that the same procedures were applied as mentioned above.

Crystal structure determination for complexes 2 and 3·OTf. X-ray diffraction data were collected at 100(2) K with graphite-monochromated Mo Kα radiation (λ = 0.71073 Å) using a narrow ω rotation (0.3º) on Bruker SMART diffractometers. The intensities were integrated by using the SAINT+ program[58] and corrected for absorption effects with the SADABS program[59] integrated in the APEX2 package. The structures were solved by the Patterson's method with SHELXS-2013[60] and refined by full-matrix least-squares methods on F^2 with SHELXL-2014[61] included in the WINGX package.[62]

Crystal data for [Ir(cod){(MeIm)$_2$CHCOO}]·2CH$_3$OH (2·2CH$_3$OH). $C_{20}H_{31}IrN_4O_4$, M_r = 583.69, monoclinic, $P2_1/n$, a=10.3999(5) Å, b=14.5133(7) Å, c=14.2006(7) Å, β=98.9050(10)º, V=2117.56(18) Å^3, Z=4, ρ_{calc}=1.831 g·cm^{-3}, μ=6.339 mm^{-1}, F(000)=1152, 0.200x0.250x0.300 mm, $2\theta_{max}$=57.330º, −13≤h≤13, −19≤k≤18, −18≤l≤18, reflections collected/unique 24437/5102 [R(int) = 0.0297], data/restraints/parameters 5102/0/293, GOF 1.028, final R indices for $I>2\sigma(I)$: R_1=0.0226, $wR2$=0.0535, R indices for all data: R_1=0.0330, $wR2$=0.0577, largest diff. peak and hole 1.594 and −0.727 e·Å^{-3}.

Crystal data for [IrH(cod){(MeIm)$_2$CHCOO}]OTf (3·OTf). $C_{19}H_{24}F_3IrN_4O_5S$, M_r=669.68, monoclinic, $P2_1/c$, a=8.8790(3) Å, b=16.9895(6) Å, c=14.9656(6) Å, β=103.14º, V=2198.46(14) Å^3, Z=4, ρ_{calc}=2.023 g·cm^3, μ=6.234 mm^{-1}, F(000)=1304, 0.110x0.120x0.200 mm, $2\theta_{max}$=57.382º, −11≤h≤11, −22≤k≤22, −20≤l≤19, reflections collected/unique 25414/5325 [R(int) = 0.0276], data/restraints/parameters 5325/1/371, GOF 1.051, final R indices for $I>2\sigma(I)$: R_1=0.0193, $wR2$=0.0430, R indices for all data: R_1=0.0230, $wR2$=0.0447, largest diff. peak and hole 1.1764 and −0.479 e·Å^{-3}.

CCDC-1545126 (**2**) and 1545127 (**3·OTf**) contain the supplementary crystallographic data for this paper. These data can be obtained free of charge from The Cambridge Crystallographic Data Centre via www.ccdc.cam.ac.uk/data_request/cif.

ASSOCIATED CONTENT

Supporting Information.

NMR spectra for the new compounds and reactivity studies. Detailed information on the determination of activation parameters for the hydrogenation of CO_2. Hydrogen bonds in the molecular structure of **2**. Electronic energy, enthalpy, free energy and optimized coordinates for catalytic intermediates and transition states.

The Supporting Information is available free of charge on the ACS Publications website.

AUTHOR INFORMATION

Corresponding Author

* E-mail for J.J.P-T.: perez@unizar.es. E-mail for W.L.: Leitner@itmc.rwth-aachen.de

ORCID

Markus Hölscher: 0000-0003-4088-8924
M. Victoria Jiménez: 0000-0002-0545-9107
Walter Leitner: 0000-0001-6100-9656
Vincenzo Passarelli: 0000-0002-1735-6439
Jesús J. Pérez-Torrente: 0000-0002-3327-0918

Notes

The authors declare no competing financial interest.

ACKNOWLEDGMENT

Financial support from the Ministerio de Economía y Competitividad (MINECO/FEDER) of Spain (Projects CTQ2013-42532-P and CTQ2016-75884-P) and Diputación General de Aragón (DGA/FSE E07) is gratefully acknowledged. R. P-O. acknowledges her fellowship from MINECO (BES-2011-045364, EEBB-I-14-08939 and EEBB-I-15-10125). Additional support from the DFG (Cluster of Excellence "Tailor-made Fuels from Biomass", which is funded by the Excellence initiative by the German Federal and State Governments to promote science and research at German universities) is gratefully acknowledged.

REFERENCES

[1] Reutemann, W.; Kieczka, H. Formic Acid. In *Ullmann's Encyclopedia of Industrial Chemistry*, Wiley-VCH: Weinheim, Germany, **2011**.

[2] a) Boddien, A.; Gaertner, F.; Mellmann, D.; Sponholz, P.; Junge, H.; Laurency, G.; Beller, M. *CHIMIA* **2011**, *65*, 214–218. b) Johnson, T. C.; Morris, D. J.; Wills, M. *Chem. Soc. Rev.* **2010**, *39*, 81–88. c) Rice, C.; Ha, R. I.; Masel, R. I.; Waszczuk, P.; Wieckowski, A.; Barnard, T. *J. Power Sources* **2002**, *111*, 83–89.

[3] a) Klankermayer, J.; Leitner, W. *Phil. Trans. R. Soc. A* **2016**, *374*, DOI: 10.1098/rsta.2015.0315. b) Aresta, M.; Dibenedetto, A.; Angelini, A. *Chem. Rev.* **2014**, *114*, 1709–1742. c) Centi, G.; Quadrelli, E. A.; Perathoner, S. *Energy Environ. Sci.* **2013**, *6*, 1711–1731. d) Peters, M.; Köhler, B.; Kuckshinrichs, W.; Leitner, W.; Markewitz, P.; Müller, T. E. *ChemSusChem* **2011**, *4*, 1216–1240.

[4] a) Jessop, P. G. Homogeneous Hydrogenation of Carbon Dioxide. In *The handbook of homogeneous hydrogenation*, de Vries, J. G.; Elsevier, C. J. (Ed.), Wiley-VCH: Weinheim, Germany, 2007. p 489. b) Klankermayer, J.; Wesselbaum, S.; Beydoun, K.; Leitner, W. *Angew. Chem. Int. Ed.* **2016**, *55*, 7296–7343. c) Wang, W.-H.; Himeda, Y.; Muckerman, J. T.; Manbeck, G. F.; Fujita, E. *Chem. Rev.* **2015**, *115*, 12936–12973. d) Himeda, Y.; Miyazawa, S.; Hirose, T. *ChemSusChem* **2011**, *4*, 487–493.

[5] For early reviews, see: a) Leitner, W. *Angew. Chem., Int. Ed. Engl.* **1995**, *34*, 2207–2221. b) Jessop, P. G.; Ikariya, T.; Noyori, R. *Chem. Rev.* **1995**, *95*, 259–272.

[6] a) Daw, P.; Chakraborty, S.; Leitus, G.; Diskin-Posner, Y.; Ben-David, Y.; Milstein, D. *ACS Catal.* **2017**, *7*, 2500–2504. b) Affan, M. A.; Jessop. P. G. *Inorg. Chem.* **2017**, 10.1021/acs.inorgchem.7b01242. c) Tlili, A.; Blondiaux, E.; Frogneux, X.; Cantat. T. *Green Chem.* **2015**, *17*, 157–168. d) Fernández-Alvarez, F. J.; Aitanib, A. M.; Oro, L. A.; *Catal. Sci. Technol.* **2014**, *4*, 611–624. e) Federsel, C.; Boddien, A.; Jackstell, R.; Jennerjahn, R.; Dyson, P. J.; Scopelliti, R.; Laurenczy, G.; Beller, M. *Angew. Chem. Int. Ed.* **2010**, *49*, 9777–9780.

[7] a) Li, Y.; Sorribes, I.; Yan, T.; Junge, K.; Beller, M. *Angew. Chem. Int. Ed.* **2013**, *52*, 12156–12160. b) Beydoun, K.; vom Stein, T.; Klankermayer, J.; Leitner, W. *Angew. Chem. Int. Ed.* **2013**, *52*, 9554–9557.

[8] a) Rohmann, K.; Kothe, J.; Haenel, M. W.; Englert, U.; Hölscher, M.; Leitner, W. *Angew. Chem. Int. Ed.* **2016**, *55*, 8966–8969. b) Moret, S.; Dyson, P. J.; Laurenczy, G. *Nat. Commun.* **2014**, *5*, 1–7.

[9] a) Rawat, K. S.; Mahata, A.; Choudhuri, I.; Pathak, B. *J. Phys. Chem. C* **2016**, *120*, 16478–16488. b) Mondal, B.; Neese, F.; Ye. S. *Inorg. Chem.* **2015**, *54*, 7192–7198.

[10] Elek, J.; Nádasdi, L.; Papp, G.; Laurenczy, G.; Joó, F. *Appl. Catal. A. General*, **2003**, *255*, 5967.

[11] Inoue, Y.; Izumida, H.; Sasaki, Y.; Hashimoto, H. *Chem. Lett.*, **1976**, 863–864.

[12] a) Dong, K.; Razzaq, R.; Hu, Y.; Ding, K. *Top. Curr. Chem.* **2017**, *375*,1. doi:10.1007/s41061-017-0107-x. b) Wang, W.-H.; Himeda, Y. Recent Advances in Transition Metal-Catalyzed Homogeneous Hydrogenation of Carbon Dioxide in Aqueous Media. In *Hydrogenation*, Karamé, I. (Ed.), InTech, **2012**, DOI: 10.5772/48658.

[13] a) Wang, W.-H. Muckerman, J. T.; Fujita, E.; Himeda, Y.; *ACS Catal.* **2013**, *3*, 856–860. b) Hull, J. F.; Himeda, Y.; Wang, W.-H.; Hashiguchi, B.; Periana, R.; Szalda, D. J.; Muckerman, J. T.; Fujita, E. *Nature Chem.* **2012**, *4*, 383–388. c) Wang, W. -H.; Hull, J. F.; Muckerman, J. T.; Fujita, E.; Himeda, Y. *Energy Environ. Sci.* **2012**, *5*, 7923–7926. d) Himeda Y., *Eur. J. Inorg. Chem.* **2007**, 3927–3941.

[14] a) Tanaka, R.; Yamashita, M.; Nozaki, K. *J. Am. Chem. Soc.* **2009**, *131*, 14168–14169. b) Tanaka, R.; Yamashita, M.; Chung, L. W.; Morokuma, K.; Nozaki, K. *Organometallics* **2011**, *30*, 6742–6750.

[15] Schmeier, T. J.; Dobereiner, G. E.; Crabtree, R. H.; Hazari, N. *J. Am. Chem. Soc.* **2011**, *133*, 9274–9277.

[16] Liu, C.; Xie, J.-H.; Tian, G.-L.; Li, W.; Zhou, Q.-L. *Chem. Sci.* **2015**, *6*, 2928–2931.

[17] a) Khusnutdinova, J. R.; Milstein, D. *Angew. Chem. Int. Ed.* **2015**, *54*, 12236–12273. b) Gunanathan, C.; Milstein, D. *Acc. Chem. Res.* **2011**, *44*, 588–602.

[18] a) Vogt, M.; Gargir, M.; Iron, M. A.; Diskin-Posner, Y.; Ben-David, Y.; Milstein, D. *Chem. Eur. J.* **2012**, *18*, 9194–9197. b) Huff, C. A.; Kampf, J. W.; Sanford, M. S. *Organometallics* **2012**, *31*, 4643–4645.

[19] Huff, C. A.; Sanford, M. S. *ACS Catal.* **2013**, *3*, 2412–2416.

[20] a) Filonenko, G. A.; Hensen, E. J. M.; Pidko, E. A. *Catal. Sci. Technol.* **2014**, *4*, 3474–3485. b) Filonenko, G. A.; van Putten, R.; Schulpen, E. N.; Hensen, E. J. M.; Pidko, E. A. *ChemCatChem* **2014**, *6*, 1526–1530. c) Filonenko, G. A.; Conley, M. P.; Copéret, C.; Lutz, M.; Hensen, E. J. M.; Pidko, E. A. *ACS Catal.* **2013**, *3*, 2522–2526.

[21] a) Hopkinson, M. N.; Richter, C.; Schedler, M.; Glorius, F. *Nature*, **2014**, *510*, 485–496. b) Benhamou, L.; Chardon, E.; Lavigne, G.; Bellemin-Laponnaz, S.; César, V. *Chem. Rev.* **2011**, *111*, 2705–2733. c) Hahn, F. E.; Jahnke, M. C. *A ngew. Chem. Int. Ed.* **2008**, *47*, 3122–3172. d) Peris E. *Top. Organomet. Chem.* **2007**, *21*, 83–116. e) Herrmann, W. A. *Angew. Chem. Int. Ed.* **2002**, *41*, 1290–1309.

[22] a) Azua, A.; Sanz, S.; Peris, E. *Chem. Eur. J.* **2011**, *17*, 3963–3967. b) Sanz, S.; Benitez, M.; Peris, E. *Organometallics* **2010**, *29*, 275–277. c) Sanz, S.; Azua, A.; Peris, E. *Dalton Trans.* **2010**, *39*, 6339–6343.

[23] Siek, S.; Burks, D. B.; Gerlach, D. L.; Liang, G.; Tesh, J. M.; Thompson, C. R.; Qu, F.; Shankwitz, J. E.; Vasquez, R. M.; Chambers, N.; Szulczewski, G. J.; Grotjahn, D. B.; Webster, C. E.; Papish. E. T. *Organometallics* **2017**, *36*, 1091–1106.

[24] a) Filonenko, G. A.; Smykowski, D.; Szyja, B. M.; Li, G.; Szczygieł, J.; Hensen, E. J. M.; Pidko, E. A. *ACS Catal.* **2015**, *5*, 1145–1154. b) Filonenko, G. A.; Cosimi, E.; Lefort, L.; Conley, M. P.; Coperet, C.; Lutz, M.; Hensen, E. J. M.; Pidko, E. A. *ACS Catal.* **2014**, *4*, 2667–2671.

[25] a) Jiménez, M. V.; Fernández-Tornos, J.; Modrego, F. J.; Pérez-Torrente, J. J.; Oro, L. A. *Chem. Eur. J.* **2015**, *21*, 17877–17889. b) Jiménez, M. V.; Fernández-Tornos, J.; Pérez-Torrente, J. J.; Modrego, F. J.; García-Orduña, Pilar.; Oro, L. A. *Organometallics* **2015**, *34*, 926–940. c) Jiménez, M. V.; Fernández-Tornos, J.; Pérez-Torrente, J. J.; Modrego, F. J.; Winterle, S.; Cunchillos, C.; Lahoz, F.; Oro, L. A. *Organometallics* **2011**, *30*, 5493–5508. d) Jiménez, M. V.; Pérez-Torrente, J. J.; Bartolomé, M. I.; Gierz, V.; Lahoz, F. J.; Oro, L. A. *Organometallics* **2008**, *27*, 224–234.

[26] a) Fei, Z.; Ang, W. H.; Zhao, D.; Scopelliti, R.; Zvereva, E. E.; Katsyuba, S. A.; Dyson, P. J. *J. Phys. Chem. B* **2007**, *111*, 10095–10108. b) Wasserscheid, P.; Welton, T. In *Ionic Liquids in Synthesis*, Wiley-VCH: Weinheim, Germany, 2003.

[27] a) Carey, F. A.; Sundberg, R. J. In Advanced Organic Chemistry, Springer: New York, 2007; b) Ho, T.-L.; Olah, G. A. *Proc. Natl. Acad. Sci.* **1978**, *75*, 4–6, and references therein.

[28] a) Peris, E. Routes to N-Heterocyclic Carbene Complexes, In *Top. Organomet. Chem.*; Glorius, F. (Ed.), Springer: New York, USA, 2007, 21, 83–116. b) Aznarez, F.; Sanz Miguel, P. J.; Tan, T. T. Y.; Hahn, F. E. *Organometallics* **2016**, 35, 410–419. c) Aznarez, F.; Iglesias, M.; Hepp, A.; Veit, B.; Sanz Miguel, P. J.; Oro, L. A.; Jin, G.-X.; Hahn, F. E. *Eur. J. Inorg. Chem.* **2016**, 4598–4603.

[29] Leung, C. H.; Incarvito, C. D.; Crabtree, R. H. *Organometallics* **2006**, *25*, 6099–6107.

[30] a) Brill, M.; Marrwitz, D.; Rominger, F.; Hofmann, P. *J. Organomet. Chem.* **2015**, *775*, 137–151; b) Huffer, A.; Jeffery, B.; Waller, B. J.; Danopoulos, A. A. *C. R. Chimie* **2013**, *16*, 557–565.

[31] Viciano, M.; Mas-Marzá, E.; Poyatos, M.; Sanaú, M.; Crabtree, R. H.; Peris, E. *Angew. Chem. Int. Ed. Engl.* **2005**, *44*, 444–447.

[32] Nguyen, D. H.; Pérez-Torrente, J. J.; Jiménez, M. V.; Modrego, F. J.; Gómez-Bautista, D.; Lahoz, F. J.; Oro, L. A. *Organometallics* **2013**, *32*, 6918–6930.

[33] Munshi, P.; Main, A. D.; Linehan, J. C.; Tai, C.-C.; Jessop, P. G. *J. Am. Chem. Soc.* **2002**, *124*, 7963–7971.

[34] a) Tolman, W. B. Activation of small molecules. In *Organometallic and bioinorganic perspectives*, Wiley-VCH: Weinheim, Germany, **2006**. b) Fechete, I.; Vedrine, J. *Molecules* **2015**, *20*, 5638–5666.

[35] a) Chatterjee, D.; Sarkar, P. *J. Coord. Chem*. **2016**, *69*, 650–655. b) Surface, J. A.; Skemer, P.; Hayes, S. E.; Conradi, M. S. *Environ. Sci. Technol*. **2013**, *47*, 119–125. c) Moret, S.; Dyson, P. J.; Laurenczy, G. *Dalton Trans.* **2013**, *42*, 4353–4356. d) Seravalli, J.; Ragsdale, S. W. *Biochemistry* **2008**, *47*, 6770–6781. e) Mani, F.; Peruzzini, M.; Stoppioni, P. *Green Chem*. **2006**, *8*, 995–1000. f) Banyai, I.; Glaser, J.; Micskei, K.; Toth, I.; Zekany, L. *Inorg. Chem*. **1995**, *34*, 3785–3796.

[36] *CRC Handbook of Chemistry and Physics, 84th Ed.*, Lide, D. R. (Ed.), CRC Press LLC: Boca Raton, 2003.

[37] a) Langer, J.; Imhof, W.; Fabra, M. J.; García-Orduña, P.; Görls, H.; Lahoz, F. J.; Oro, L. A.; Westerhausen, M. *Organometallics* **2010**, *29*,1642–1651. b) Lee, D. W.; Jensen, C. M.; Morales-Morales, D. *Organometallics* **2003**, *22*, 4744–4749. c) Fernández-Alvarez, F. J.; Iglesias, M.; Oro, L. A.; Polo, V. *ChemCatChem* **2013**, *5*, 3481–3494.

[38] a) Nguyen, D. H.; Greger, I.; Pérez-Torrente, J. J.; Jiménez, M. V.; Modrego, F. J.; Lahoz, F. J.; Oro, L. A. *Organometallics* **2013**, *32*, 6903–6917; b) Nguyen, D. H.; Pérez-Torrente, J. J.; Lomba, L.; Jiménez, M. V.; Lahoz, F. J.; Oro, L. A. *Dalton Trans*. **2011**, *40*, 8429–8435.

[39] For a related hydride transfer from rhodium to a coordinated 1,5-cyclooctadiene ligand leading to a η^3-cyclooctenyl complex see: Gassner, F.; Dinjus, E.; Görls, H.; Leitner, W. *Organometallics* **1996**, *15*, 2078–2082.

[40] a) Jiménez, M. V.; Fernández-Tornos, J.; Pérrez-Torrente, J. J.; Modrego, F. J.; García-Orduña, P.; Oro, L. A. *Organometallics* **2015**, *34*, 926–940. b) Lee, D. W.; Jensen, C M.; Morales-Morales, D. *Organometallics* **2003**, *22*, 4744–4749.

[41] Palacios, L.; Di Giuseppe, A.; Opalinska, A.; Castarlenas, R.; Pérez-Torrente, J. J.; Lahoz, F. J.; Oro, L. A. *Organometallics* **2013**, *32*, 2768–2774.

[42] a) *The handbook of homogeneous hydrogenation*, Wiley-VCH: Weinheim, **2007**. b) Leitner, W.; Dinjus, E.; Gaßner, F. *J. Organomet. Chem*. **1994**, *475*, 257–266.

[43] a) Osadchuk, I.; Tamm, T.; Ahlquist, M. S. G. *Organometallics* **2015**, *34*, 4932–4940. b) Wesselbaum, S.; Moha, V.; Meuresch, M.; Brosinski, S.; Thenert, K. M.; Kothe, J.; Vom Stein, T.; Englert, U.; Hölscher, M.; Klankermayer, J.; Leitner, W. *Chem. Sci.* **2015**, *6*, 693–704. c) Hou, C.; Jiang, J.; Zhang, S.; Wang, G.; Zhang, Z.; Ke, Z.; Zhao, C. *ACS Catal*. **2014**, *4*, 2990–2997. d) Cao, L.; Sun, C.; Sun, N.; Meng, L.; Chen, D. *Dalton Trans*. **2013**, *42*, 5755–5763. e) Yang, X. *ACS Catal*. **2011**, *1*, 849–854. f) Ogo, S.; Kabe, R.; Hayashi, H.; Harada, R.; Fukuzumi, S. *Dalton Trans*. **2006**, *56*, 4657–4663. g) Ng, S. M.; Yin, C.; Yeung, C. H.; Chan, T. C.; Lau, C. P. *Eur. J. Inorg. Chem*. **2004**, 1788–1793.

[44] Kang, P.; Cheng, C.; Chen, Z.; Schauer, C. K.; Meyer, T. J.; Brookhart, M. *J. Am. Chem. Soc*. **2012**, *134*, 5500–5503.

[45] a) Hutschka, F.; Dedieu, A.; Eichberger, M.; Fornika, R.; Leitner, W. *J. Am. Chem. Soc*. **1997**, *119*, 4432-4443. b) Hutschka, F.; Dedieu, A.; Leitner, W. *Angew. Chem. Int. Ed. Engl*. **1995**, *34*, 1742–1745.

[46] a) Truscott, B. J.; Nelson, D. J.; Slawin, A. M. Z.; Nolan. S. P. *Chem. Commun*. **2014**, 50, 286–288. b) Truscott, B. J.; Nelson, D. J.; Lujan, C.; Slawin,. A. M. Z.; Nolan, S. P. *Chem. Eur. J.* **2013**, *19*, 7904–7916.

[47] Herde, J. L.; Lambert, J. C.; Senoff, C. V.; Cushing, M. A.; *Inorg. Synth*. **1974**, *15*, 18–20.

[48] Usón, R.; Oro, L. A.; Cabeza, J. A.; Bryndza, H. E.; Stepro, M. P. *Inorg. Synth*. **1985**, *23*, 126–130.

[49] Quezada, C.; Garrison, J. C.; Tessier, C. A.; Youngs, W. J. *J. Organomet. Chem*. **2003**, *671*, 183–186.

[50] Frey, D.; Rentzsch, C. F.; von Preysing, D.; Scherg, T.; Mühlhofer, M.; Herdtweck, E.; Herrmann, W. A. *J. Organomet. Chem*. **2006**, *691*, 5725–5738.

[51] *Gaussian 09, Revision A.1*, Frisch, M. J.; Trucks, G. W.; Schlegel, H. B.; Scuseria, G. E.; Robb, M. A.; Cheeseman, J. R.; Scalmani, G.; Barone, V.; Mennucci, B.; Petersson, G. A.; Nakatsuji, H.; Caricato, M.; Li, X.; Hratchian, H. P.; Izmaylov, A. F.; Bloino, J.; Zheng, G.; Sonnenberg, J. L.; Hada, M.; Ehara, M.; Toyota, K.; Fukuda, R.; Hasegawa, J.; Ishida, M.; Nakajima, T.; Honda, Y.; Kitao, O.; Nakai, H.; Vreven, T.; Montgomery, Jr., J. A.; Peralta, J. E.; Ogliaro, F.; Bearpark, M.; Heyd, J. J.; Brothers, E.; Kudin, K. N.; Staroverov, V. N.; Kobayashi, R.; Normand, J.; Raghavachari, K.; Rendell, A.; Burant, J. C.; Iyengar, S. S.; Tomasi, J.; Cossi, M.; Rega, N.; Millam, N. J.; Klene, M.; Knox, J. E.; Cross, J. B.; Bakken, V.; Adamo, C.; Jaramillo, J.; Gomperts, R.; Stratmann, R. E.; Yazyev, O.; Austin, A. J.; Cammi, R.; Pomelli, C.; Ochterski, J. W.; Martin, R. L.; Morokuma, K.; Zakrzewski, V. G.; Voth, G. A.; Salvador, P.; Dannenberg, J. J.; Dapprich, S.; Daniels, A. D.; Farkas, Ö.; Foresman, J. B.; Ortiz, J. V.; Cioslowski, J.; Fox, D. J. *Gaussian, Inc.*, Wallingford CT, **2009**.

[52] a) Kulkarni, A. D.; Truhlar, D. G. *J. Chem. Theory Comput*. **2011**, *7*, 2325–2332. b) Averkiev, B. B.; Zhao, Y.; Truhlar, D. G. *J. Mol. Catal. A: Chem*. **2010**, *324*, 80–88. c) Cramer, C. J.; Truhlar, D. G. *Phys. Chem. Chem. Phys*. **2009**, *11*, 10757–10816. d) Zhao, Y.; Truhlar, D. G. *J. Chem. Phys*. **2006**, *125*, 194101.

[53] a) Weigend, F.; Ahlrichs, R. *Phys. Chem. Chem. Phys*. **2005**, *7*, 3297–3305. b) Weigend, F.; Furche, F.; Ahlrichs, R. *J. Chem. Phys*. **2003**, *119*, 12753–12762. c) Eichkorn, K.; Weigend, F.; Treutler, O.; Ahlrichs, R. *Theor. Chem. Acc*. **1997**, *97*, 119–124. d) Schäfer, A.; Huber, C.; Ahlrichs, R. *J. Chem. Phys*. **1994**, *100*, 5829–5835. e) Schäfer, A.; Horn, H.; Ahlrichs, R. *J. Chem. Phys*. **1992**, *97*, 2571.

[54] a) Metz, B.; Stoll, H.; Dolg, M. *J. Chem. Phys.* **2000**, *113*, 2563–2569. b) Andrae, D.; Häußermann, U.; Dolg, M.; Stoll, H.; Preuß, H. *Theoret. Chim. Acta* **1990**, *77*, 123–141.

[55] a) Dunlap, B. I. *J. Mol. Struc. Theochem.* **2000**, *529*, 37–40. b) Dunlap, B. I. *J. Chem. Phys.* **1983**, *78*, 3140–3142.

[56] a) Marenich, A. V.; Cramer, C. J.; Truhlar, D. G. *J. Phys. Chem. B* **2009**, *113*, 6378–6396. b) Tomasi, J.; Mennucci, B.; Cammi, R. *Chem. Rev.* **2005**, *105*, 2999–3093. c) Cancès, E.; Mennucci, B.; Tomasi, J. *J. Chem. Phys.* **1997**, *107*, 3032–3041.

[57] a) Sieffert, N.; Bühl, M. *Inorg. Chem.* **2009**, *48*, 4622–4624. b) Martin, R. L.; Hay, P. J.; Pratt, L. R. *J. Phys. Chem. A* **1998**, *102*, 3565–3573.

[58] *SAINT+*, version 6.01: Area-Detector Integration Software, Bruker AXS, Madison, WI, **2001**.

[59] a) Blessing, R. H. *Acta Crystallogr. A* **1995**, *51*, 33–38. b) *SADABS*, Area Detector Absorption Correction Program, Bruker AXS, Madison, WI, **1996**.

[60] a) Sheldrick, G. M. *Acta Crystallogr. A* **1990**, *46*, 467–473;
b) Sheldrick, G. M. *Acta Crystallogr. A* **2008**, *64*, 112–122.
[61] Sheldrick, G. M. *Acta Crystallogr. C* **2015**, *71*, 3–8.
[62] Farrugia, L. J. *J. Appl. Crystallogr.* **2012**, *45*, 849–854.

Table of Contents artwork

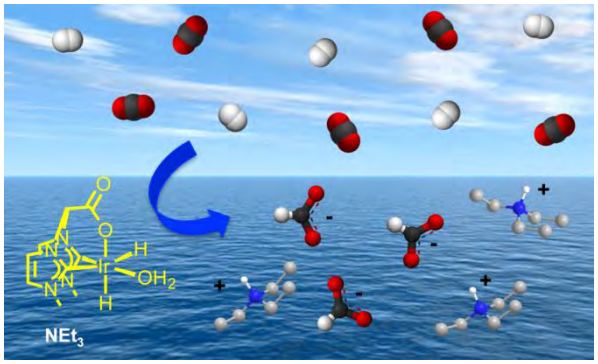

Double-Column Figures

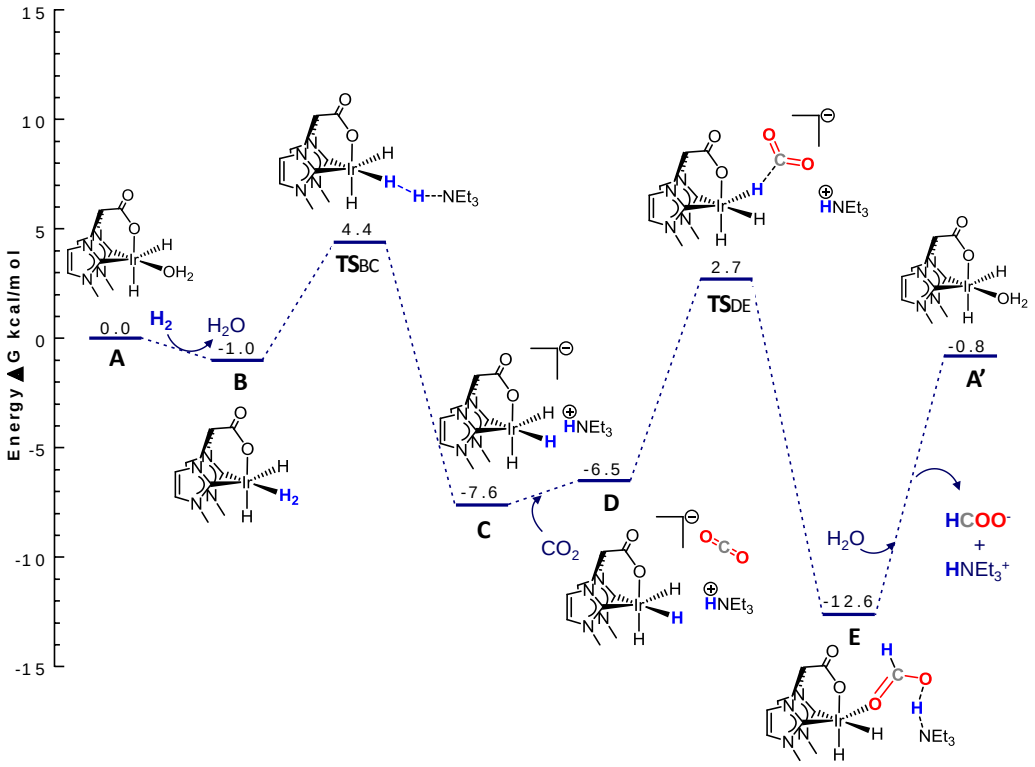

Figure 4. DFT calculated Gibbs free energy profile for the hydrogenation of CO_2 catalyzed by $[IrH_2(H_2O)\{(MeIm)_2CHCOO\}]$ in water via amine-assisted heterolytic H_2 cleavage (base-involved mechanism).

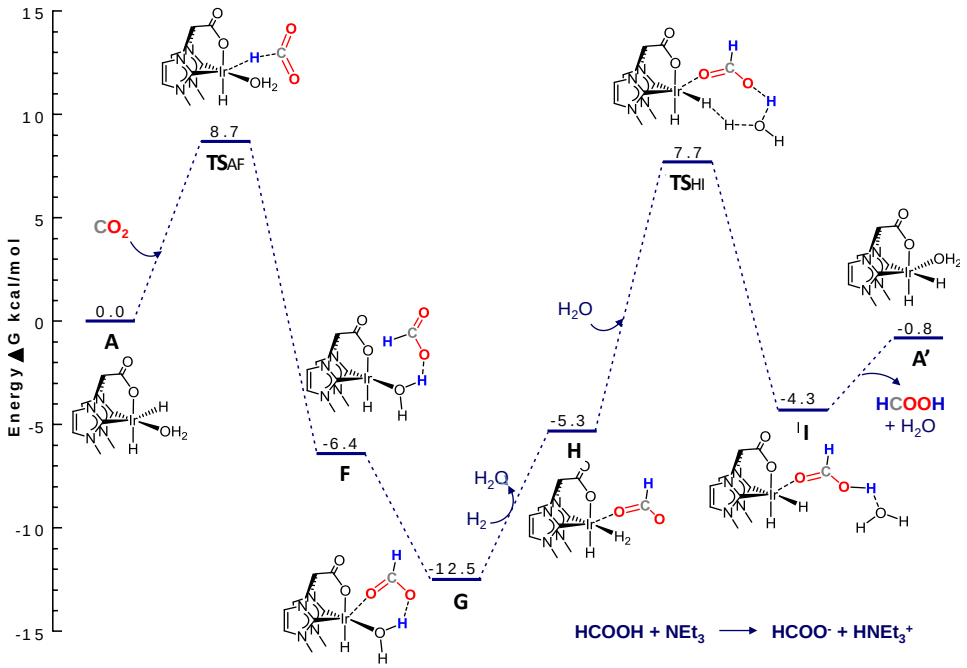

Figure 5. DFT calculated Gibbs free energy profile for the hydrogenation of CO_2 catalyzed by $[IrH_2(H_2O)\{(MeIm)_2CHCOO\}]$ in water via water-assisted heterolytic H_2 cleavage (base-free mechanism).